Evolution of Antibody Immunity to SARS-CoV-2

Christian Gaebler[1*], Zijun Wang[1*], Julio C. C. Lorenzi[1*], Frauke Muecksch[2*], Shlomo Finkin[1*], Minami Tokuyama[3*], Alice Cho[1*], Mila Jankovic[1*], Dennis Schaefer-Babajew[1*], Thiago Y. Oliveira[1*], Melissa Cipolla[1*], Charlotte Viant[1], Christopher O. Barnes[4], Yaron Bram[5], Gaëlle Breton[1], Thomas Hägglöf[1], Pilar Mendoza[1], Arlene Hurley[6], Martina Turroja[1], Kristie Gordon[1], Katrina G. Millard[1], Victor Ramos[1], Fabian Schmidt[2], Yiska Weisblum[2], Divya Jha[3], Michael Tankelevich[3], Gustavo Martinez-Delgado[3], Jim Yee[7], Roshni Patel[1], Juan Dizon[1], Cecille Unson-O'Brien[1], Irina Shimeliovich[1], Davide F. Robbiani[8], Zhen Zhao[7], Anna Gazumyan[1], Robert E. Schwartz[5,9], Theodora Hatziioannou[2], Pamela J. Bjorkman[4], Saurabh Mehandru[3,#], Paul D. Bieniasz[2,10,#], Marina Caskey[1,#], Michel C. Nussenzweig[1,10,#]

[1]Laboratory of Molecular Immunology, The Rockefeller University, New York, NY 10065, USA.

[2]Laboratory of Retrovirology, The Rockefeller University, New York, NY 10065, USA.

[3] Division of Gastroenterology, Department of Medicine, Icahn School of Medicine at Mount Sinai, New York, NY 10029, USA.

[4] Division of Biology and Biological Engineering, California Institute of Technology, Pasadena, CA, USA.

[5] Division of Gastroenterology and Hepatology, Department of Medicine, Weill Cornell Medicine, New York, NY 10065, USA.

[6] Hospital Program Direction, The Rockefeller University, New York, NY 10065, USA.

[7] Department of Pathology and Laboratory Medicine, Weill Cornell Medicine, New York, NY 10065, USA.

24 [8] Institute for Research in Biomedicine, Università della Svizzera italiana, Bellinzona,
25 Switzerland.
26 [9] Department of Physiology, Biophysics and Systems Biology, Weill Cornell Medicine, New
27 York, NY 10065, USA.
28 [10] Howard Hughes Medical Institute
29
30 [*]Equal contribution
31
32 [#]Send correspondence to Saurabh Mehandru: saurabh.mehandru@mssm.edu, Paul D. Bieniasz:
33 pbieniasz@rockefeller.edu, Marina Caskey: mcaskey@rockefeller.edu, or Michel C.
34 Nussenzweig: nussen@rockefeller.edu
35

Severe acute respiratory syndrome coronavirus-2 (SARS-CoV-2) has infected 78 million individuals and is responsible for over 1.7 million deaths to date. Infection is associated with development of variable levels of antibodies with neutralizing activity that can protect against infection in animal models. Antibody levels decrease with time, but the nature and quality of the memory B cells that would be called upon to produce antibodies upon re-infection has not been examined. Here we report on the humoral memory response in a cohort of 87 individuals assessed at 1.3 and 6.2 months after infection. We find that IgM, and IgG anti-SARS-CoV-2 spike protein receptor binding domain (RBD) antibody titers decrease significantly with IgA being less affected. Concurrently, neutralizing activity in plasma decreases by five-fold in pseudotype virus assays. In contrast, the number of RBD-specific memory B cells is unchanged. Memory B cells display clonal turnover after 6.2 months, and the antibodies they express have greater somatic hypermutation, increased potency and resistance to RBD mutations, indicative of continued evolution of the humoral response. Analysis of intestinal biopsies obtained from asymptomatic individuals 4 months after coronavirus disease-2019 (COVID-19) onset, using immunofluorescence, or polymerase chain reaction, revealed persistence of SARS-CoV-2 nucleic acids and immunoreactivity in the small bowel of 7 out of 14 volunteers. We conclude that the memory B cell response to SARS-CoV-2 evolves between 1.3 and 6.2 months after infection in a manner that is consistent with antigen persistence.

56 Antibody responses to SARS-CoV-2 were initially characterized in a cohort of COVID-19-
57 convalescent individuals approximately 40 days (1.3 months) after infection [1]. Between 31
58 August and 16 October 2020, 100 participants returned for a 6-month follow-up study visit.
59 Although initial criteria allowed enrollment of close contacts of individuals diagnosed with
60 reverse transcription (RT–PCR) confirmed SARS-CoV-2 infection [1], 13 of the contacts did not
61 seroconvert and were excluded from further analyses. The remaining 87 participants with RT-
62 PCR–confirmed COVID-19 diagnosis and/or seroconversion returned for analysis approximately
63 191 days (6.2 months, range: 165-223 days) after the onset of symptoms. In this cohort,
64 symptoms lasted for a median of 12 days (0–44 days) during the acute phase, and 10 (11%) of
65 the participants were hospitalized. Consistent with other reports [2,3], 38 (44%) of the participants
66 reported persistent long-term symptoms attributable to COVID-19 (Methods and Supplementary
67 Tables 1 and 2). The duration and severity of symptoms during acute disease was significantly
68 greater among participants with persistent post-acute symptoms at the second study visit
69 (Extended Data Fig. 1m-q). Importantly, all 87 participants tested negative for SARS-CoV-2 at
70 the 6-month follow-up study visit using an approved saliva-based PCR assay (Methods).
71 Participant demographics and clinical characteristics are shown in Supplementary Tables 1,2.
72
73 Antibody reactivity in plasma to RBD and nucleoprotein (N) was measured by enzyme-linked
74 immunosorbent assay (ELISA) and automated serological assays [1,4,5]. Anti-RBD assays were
75 strongly correlated (ELISA anti-RBD IgG and IgM/Pylon-IgG and IgM at 1.3 months, $r=0.9200$
76 and $r=0.7543$, $p < 0.0001$, respectively. Extended Data Fig 2a-d) while anti-N assays showed a
77 moderate correlation (anti-N IgG ELISA and Roche anti-N total Ig at 1.3 months, $r=0.3596$, $p =$
78 0.0012. Extended Data Fig 2e-f). The anti-RBD and ELISA anti-N antibodies in plasma

79 decreased significantly between 1.3 and 6.2 months (Fig. 1a-d). Notably, the decreased binding
80 activity differed significantly by isotype and target. IgM showed the greatest decrease in anti-
81 RBD reactivity (53%), followed by IgG (32%) while anti-RBD IgA decreased by only 15% and
82 anti-N IgG levels by 22% (Fig. 1e). In contrast, the Roche anti-N assay[5] showed a small but
83 significant increase (19%) in reactivity between the two time points (Extended Data Fig 2g)
84 which might be explained by the use of an antigen bridging approach[6]. In all cases the magnitude
85 of the decrease was inversely proportional to and directly correlated with the initial antibody
86 levels such that individuals with higher initial levels showed greater relative changes (Fig. 1f-i,
87 Extended Data Fig 2h). All measurements were strongly correlated between the two time points
88 (Extended Data Fig 2i-m) and anti-N IgG correlated with IgM, IgG and IgA anti-RBD reactivity
89 at 1.3 months, respectively (Extended Data Fig. 2n-p). Notably, individuals with persistent post-
90 acute symptoms had significantly higher anti-RBD IgG and anti-N total antibody levels at both
91 study visits (Extended Data Fig. 1a-l).
92
93 Plasma neutralizing activity was measured using an HIV-1 virus pseudotyped with the SARS-
94 CoV-2 spike protein[1,7]. Consistent with other reports the geometric mean half-maximal
95 neutralizing titer (NT_{50}) in this group of 87 participants was 401 and 78 at 1.3 and 6.2 months,
96 respectively, representing a five-fold decrease (Fig. 1j-k)[8,9]. Neutralizing activity was directly
97 correlated with the IgG anti-RBD ELISA measurements (Extended data Fig. 2q-r). Moreover,
98 the absolute magnitude of the decrease in neutralizing activity was inversely proportional to and
99 directly correlated with the neutralizing activity at the earlier time point (Fig. 1l). We conclude
100 that antibodies to RBD and plasma neutralizing activity decrease significantly but remain
101 detectable 6 months after infection with SARS-CoV-2 in the majority of individuals.

102

103 To examine the phenotypic landscape of circulating B cells we performed high-dimensional flow
104 cytometry on 41 randomly selected individuals at both time points and compared to pre-COVID-
105 19 samples from healthy individuals (n=20). Global high-dimensional mapping with t-distributed
106 stochastic neighbor embedding (tSNE) revealed significant persistent alterations in SARS-CoV-2
107 recovered individuals (Extended data Fig. 3a). The relative representation of clusters 2, 7, 8, 10
108 corresponding to naïve, memory, plasmablasts and plasma cells was decreased at 1.3 months and
109 remained so at the later time point. Metacluster 15, which corresponds to immature B cells that
110 are recent bone marrow immigrants was increased at the early time point but returned to control
111 levels at the end of the observation period (Extended data Fig. 3b-d).

112

113 Whereas plasma cells are the source of circulating antibodies, memory B cells contribute to
114 recall responses. To identify and enumerate the circulating SARS-CoV-2 memory B cell
115 compartment we used flow cytometry to isolate individual B lymphocytes with receptors that
116 bound to RBD [1] (Fig. 2a and Extended data Fig. 4). Notably, the percentage of RBD-binding
117 memory B cells increased marginally between 1.3 and 6.2 months in 21 randomly selected
118 individuals (Fig. 2b).

119

120 To determine whether there were changes in the antibodies produced by memory B cells after 6.2
121 months, we obtained 532 paired antibody heavy and light chains from the same 6 individuals that
122 were examined at the earlier time point[1] (Supplementary Table 3). There was no significant
123 difference in IGV gene representation at the two time points, including the over-representation of
124 the *IGHV3-30* and *3-53* gene segments [1,10-15] (Extended data Fig. 5a-b). In keeping with this

125 observation, and similar to the earlier time point, antibodies that shared the same IGHV and
126 IGLV genes comprised 8.6% of all sequences in different individuals (Extended data Fig. 5c). As
127 might be expected, there was a small but significant overall increase in the percentage of IgG-
128 expressing anti-RBD memory cells, from 49% to 58% ($p=0.011$, Extended data Fig. 5d-f).
129 Consistent with the fractional increase in IgG memory cells, the extent of somatic hypermutation
130 for both IGH and IGL differed significantly in all 6 individuals between the two time points.
131 Whereas the average number of nucleotide mutations in IGH and IGL was only 4.2 and 2.8 at the
132 first time point, these values were increased to 11.7 and 6.5 at the second time point ($p<0.0001$,
133 Fig. 2c and Extended data Fig. 6a-f). In contrast, the overall average IGH and IGL CDR3 length
134 and hydrophobicity were unchanged (Extended data Fig. 6g-h).
135
136 Similar to the earlier time point, we found expanded clones of memory B cells at 6.2 months
137 including 23 that appeared at both time points. However, expanded clones accounted for only
138 12.4% of all antibody sequences after 6.2 months compared to 32% after 1.3 months ($p = 0.0225$,
139 Fig. 2d-e). In addition, the overall clonal composition of the memory compartment differed at the
140 two time points in all individuals examined (Fig. 2d). Forty-three expanded clones that were
141 present at the earlier time point were not detectable after 6.2 months while 22 new expanded
142 clones appeared. In addition, the relative distribution of clones that appeared at both time points
143 also varied. For example, the dominant clones in COV21 and COV57 representing 9.0% and
144 16.7% of all sequences, respectively, were reduced to 1.1% and 1.9% of all sequences after 6.2
145 months (Fig. 2d and Supplementary Table 3). We conclude that while the magnitude of the
146 RBD-specific memory B cell compartment is conserved between 1.3 and 6.2 months after

147 SARS-CoV-2 infection, there is significant clonal turnover and antibody sequence evolution,
148 consistent with prolonged germinal center reactions.
149
150 One hundred and twenty-two representative antibodies from the 6.2-month time point were
151 tested for reactivity to RBD (Supplementary Table 4). The antibodies that were evaluated
152 included: (1) 49 that were randomly selected from those that appeared only once; (2) 23 that
153 appeared as singles at both 1.3 and 6.2 months; (3) 23 representatives of newly appearing
154 expanded clones; (4) 27 representatives of expanded clones appearing at both time points. One
155 hundred and fifteen of 122 of the antibodies bound to RBD indicating that flow cytometry
156 efficiently identified B cells producing anti-RBD antibodies (Fig. 3a and Supplementary Tables
157 4 and 5). Taking all antibodies together, the mean ELISA half-maximal effective concentration
158 (EC_{50}) was not significantly different at the two time points (Fig. 3a, Supplementary Table 4 and
159 [1]). However, comparison of the antibodies that were present at both time points revealed a
160 significant improvement of the EC_{50} after 6.2 months ($p = 0.0227$, Fig. 3b and Extended data
161 Fig.7a).
162
163 To determine whether the antibodies expressed by memory B cells at the late time point also
164 showed altered breadth, we compared them to earlier clonal relatives in binding assays using
165 control and mutant RBDs: The mutations E484K and Q493R[16] were selected for resistance to
166 class 2 antibodies such as C144 and C121 that bind directly to the ACE2 interaction ridge in the
167 RBD [1,17-19] while R346S, N439K, and N440K were selected for resistance to class 3 antibodies
168 such as C135 that do not directly interfere with ACE2 binding [1,16-19] (Fig. 3c). In addition,
169 V367F, A475V, S477N, and V483A represent circulating variants that confer complete or partial

170 resistance to class 1 and 2 antibodies [16,17,20] (Fig. 3c). Out of 52 antibody clonal pairs appearing
171 at both time points, 43 (83%) showed overall increased binding to mutant RBDs at the 6.2-month
172 time point (Extended data Fig. 7b-k, Supplementary Table 5). For example, C144, an antibody
173 recovered at the 1.3-month time point, was unable to bind to Q493R or E484K RBDs, but all 5
174 of its 6.2-month clonal derivatives bound to Q493R, and one also showed binding to E484K
175 (Fig. 3d). Overall, the most pronounced increase in binding occurred for RBD mutations in
176 amino acid positions such as E484, Q493, N439, N440 and R346 that are critical for binding of
177 class 2 and 3 antibodies [16,17] (Fig. 3e, Extended data Fig. 7b-k and Supplementary Table 5).
178
179 Next, all 122 antibodies from the 6.2 month time point were tested for activity in a pseudotyped
180 SARS-CoV-2 neutralization assay [1,7] (Fig. 4a, Supplementary Table 6). Consistent with RBD
181 binding assays, the mean neutralization half-maximal inhibitory concentrations (IC_{50}) values
182 were not significantly different at the two time points when all antibodies were compared (Fig.
183 4a and [1]). However, comparison of the antibodies that were present at both time points revealed a
184 significant improvement of the IC_{50} values at 6.2 months ($p=0.0003$, Fig. 4b and Extended data
185 Fig. 8a).
186
187 To determine whether the antibodies exhibiting altered RBD binding also show increased
188 neutralizing breadth, we tested 5 representative antibody pairs recovered at the two time points
189 against HIV-1 viruses pseudotyped with E484G, Q493R, and R346S mutant spike proteins (Fig.
190 4c, Supplementary Table 6). Notably, the Q493R and E484G pseudotyped viruses were resistant
191 to neutralization by C144; in contrast, its 6.2-month clonal derivative C051 neutralized both
192 variants with IC_{50} values of 4.7 and 3.1 ng/ml respectively (Fig. 4c-d). Similarly, R346S

193 pseudotyped viruses were resistant to C032, but a 6.2-month clonal derivative C080 neutralized
194 this variant with an IC_{50} of 5.3 ng/ml (Fig. 4c, Extended data Fig. 8b-f). Consistent with the
195 observed changes in binding and neutralizing activity several late-appearing antibodies (e.g.
196 C051) had acquired mutations directly in or adjacent to the RBD-binding paratope (Fig. 4e,
197 Extended data Fig. 8g-j). We conclude that memory B cells that evolved during the observation
198 period express antibodies with increased neutralizing potency and breadth.
199
200 Antibody evolution occurs by somatic mutation and selection in germinal centers wherein
201 antigen can be retained in the form of immune complexes on the surface of follicular dendritic
202 cells for prolonged periods of time. Residual protein in tissues represents another potential
203 source of antigen. SARS-CoV-2 replicates in ACE2-expressing cells in the lungs, nasopharynx
204 and small intestine [21-24], and viral RNA has been detected in stool samples even after the virus is
205 cleared from the nasopharynx [25-27]. To determine whether there might be antigen persistence in
206 the intestine after resolution of clinical illness, we obtained biopsies from the upper and lower
207 gastrointestinal (GI) tract of 14 individuals, an average of 4 months (range 2.8-5.7 months) after
208 initial SARS-CoV-2 diagnosis (Supplementary Table 7). Immunostaining was performed to
209 determine whether viral protein was also detectable in upper and lower GI tract, with de-
210 identified biopsies from individuals pre-dating the pandemic (n=10) serving as controls. ACE2
211 and SARS-CoV-2 N protein was detected in intestinal enterocytes in 5 of 14 individuals (Fig. 5a-
212 d, Extended data Fig. 9a-h and 10a-b, and Supplementary Table 7) but not in historic control
213 samples (Extended data Fig. 9i-l). When detected, immunostaining was sporadic, patchy,
214 exclusive to the intestinal epithelium and not associated with inflammatory infiltrates (Extended
215 data Fig. 9a-h and 10a-b). Clinically approved nasopharyngeal swab PCR assays were negative

216 in all 14 individuals at the time of biopsy. However, biopsy samples from 3 of the 14 participants
217 produced PCR amplicons that were sequence verified as SARS-CoV-2 (Methods and
218 Supplementary Table 7). In addition, viral RNA was detected by in situ hybridization in biopsy
219 samples from the two participants that were tested (Extended data Fig. 10c-d) but not in historic
220 control samples (Extended data Fig. 10e). Sampling variability during the endoscopic procedure
221 likely contributed to incomplete concordance between detection of viral RNA and protein assays.
222
223 Neutralizing antibodies to SARS-CoV-2 develop in most individuals after infection but decay
224 with time [6,8,9,28-31]. These antibodies are effective in prevention and therapy in animal models and
225 are likely to play a role in protection from re-infection in humans [32]. Although there is a
226 significant decrease in plasma neutralizing activity between 1.3 and 6.2 months, antibody titers
227 remain measurable in most individuals [8,9,28-31,33-36].
228
229 Neutralizing monoclonal antibodies obtained from individuals during the early convalescence
230 period showed remarkably low levels of somatic mutations that some investigators attributed to
231 defects in germinal center formation [10,11,13,37-40,]. Our data indicate that the anti-SARS-CoV-2
232 memory B cell response evolves during the first 6 months after infection, with accumulation of
233 Ig somatic mutations, and production of antibodies with increased neutralizing breadth and
234 potency. Persistent antibody evolution occurs in germinal centers and requires that B cells are
235 exposed to antigen trapped in the form of immune complexes on follicular dendritic cells [41]. This
236 form of antigen can be long-lived because follicular dendritic cells do not internalize immune
237 complexes. In addition, even small amounts of persistent viral antigen could fuel antibody
238 evolution. The observation that SARS-CoV-2 mRNA and protein remains detectable in the small

239 intestinal epithelium in some individuals months after infection is consistent with the relative
240 persistence of anti-RBD IgA antibodies and continued antibody evolution [34-36].
241 Memory responses are responsible for protection from re-infection and are essential for effective
242 vaccination. The observation that memory B cell responses do not decay after 6.2 months [34,35,42],
243 but instead continue to evolve, is strongly suggestive that individuals who are infected with
244 SARS-CoV-2 could mount a rapid and effective response to the virus upon re-exposure.
245

246 **Figure Legends**

247 **Fig. 1: Plasma antibody dynamics against SARS-CoV-2.**

248 **a**–**d**, Results of ELISAs measuring plasma reactivity to RBD (**a**,**b,c**) and N protein (**d**) at the
249 initial 1.3 and 6.2 month follow-up visit, respectively. **a**, Anti-RBD IgM. **b**, Anti-RBD IgG. **c**,
250 Anti-RBD IgA **d**, Anti-N IgG. The normalized area under the curve (AUC) values for 87
251 individuals are shown in **a,b,c** and **d** for both time points, respectively. Positive and negative
252 controls were included for validation [1]. **e**, Relative change in plasma antibody levels between 1.3
253 and 6.2 months for anti-RBD IgM, IgG, IgA and anti-N IgG in all 87 individuals, respectively. **f-**
254 **i,** Relative change in antibody levels between 1.3 and 6.2 months plotted against the
255 corresponding antibody levels at 1.3 months. **f**, Anti-RBD IgM. r = -0.83, p <0.0001. **g**, Anti-
256 RBD IgG. r = -0.76, p <0.0001. **h**, Anti-RBD IgA. r = -0.67, p <0.0001. **i**, Anti-N IgG. r = -0.87,
257 p <0.0001. **j.** Ranked average half-maximal inhibitory plasma neutralizing titer (NT50) at 1.3
258 months (blue) and 6.2 months (red) for the 87 individuals studied. **k.** Graph shows NT50 for
259 plasma from all 87 individuals collected at 1.3 and 6.2 months p <0.0001. **l.** Relative change in
260 plasma neutralizing titers between 1.3 and 6.2 months plotted against the corresponding titers at
261 1.3 months. For **a-e**, **k** plotted values and horizontal bars indicate geometric mean. Statistical
262 significance was determined using two-tailed Wilcoxon matched-pairs signed rank test in **a-d**, **k**
263 and Friedman with Dunn's multiple comparison test in **e**. The *r* and *p* values in **f** – **i** and **l** were
264 determined by two-tailed Spearman's correlations.

265 **Fig. 2: Anti-SARS-CoV-2 RBD antibody sequences.**

266 **a,** Representative flow cytometry plots showing dual AlexaFluor-647–RBD- and PE–RBD-
267 binding B cells for six study individuals (gating strategy is in Extended Data Fig.5). Percentage

268 of antigen-specific B cells is indicated. **b.** As in **a.** graph summarizes %RBD binding memory B
269 cells in samples obtained at 1.3 and 6.2 months from 21 randomly selected individuals. Red
270 horizontal bars indicate geometric mean values. Statistical significance was determined using
271 two-tailed Wilcoxon matched-pairs signed rank test. **c,** Number of somatic nucleotide mutations
272 in the IGVH (top) and IGVL (bottom) in antibodies obtained after 1.3 or 6.2 months from the
273 indicated individual or all six donors (right). Statistical significance was determined using two-
274 tailed Mann–Whitney U-tests and horizontal bars indicate median values. **d,** Pie charts show the
275 distribution of antibody sequences from six individuals after 1.3 [1] (upper panel) or 6.2 months
276 (lower panel). The number in the inner circle indicates the number of sequences analyzed for the
277 individual denoted above the circle. Pie slice size is proportional to the number of clonally
278 related sequences. The black outline indicates the frequency of clonally expanded sequences
279 detected in each participant. Colored slices indicate persisting clones (same IGHV and IGLV
280 genes and highly similar CDR3s) found at both timepoints in the same participant. Grey slices
281 indicate clones unique to the timepoint. White slices indicate singlets found at both timepoints,
282 while the remaining white area indicates sequences isolated once. **e.** Graph shows relative
283 clonality at both time points for all six donors. Red horizontal bars indicate mean values.
284 Statistical significance was determined using two-tailed t-test.

285 **Fig. 3: Anti-SARS-CoV-2 RBD monoclonal antibody reactivity.**

286 **a,** Graphs show anti-SARS-CoV-2 RBD antibody reactivity. ELISA EC_{50} values for all
287 antibodies measured at 1.3 [1] and 122 selected monoclonal antibodies at 6.2 months. Horizontal
288 bars indicate geometric mean. Statistical significance was determined using two-tailed Mann–
289 Whitney U-test. **b**, EC_{50} values for all 52 antibodies that appear at 1.3 and 6.2 months. Average
290 of two or more experiments. Horizontal bars indicate geometric mean. Statistical significance

291 was determined using two-tailed Wilcoxon matched-pairs signed rank test. **c,** Surface
292 representation of the RBD with the ACE2 binding footprint indicated as a dotted line and
293 selected residues found in circulating strains (grey) and residues that mediate resistance to class 2
294 (red, C144) and 3 (green, C135) antibodies highlighted as sticks. **d.** Graphs show ELISA binding
295 curves for C144 (black dashed line) and its clonal relatives obtained after 6.2 months (C050-54,
296 solid lines) binding to wild type, Q493R, R346S, and E484K mutant RBDs. **e.** Heat map shows
297 log2 relative fold change in EC_{50} against indicated RBD mutants for 26 antibody clonal pairs
298 obtained at 1.3 and 6.2 month with the most pronounced changes in reactivity. The participant
299 origin for each antibody pair is indicated above. All experiments were performed at least twice.

300 **Fig.4: Anti-SARS-CoV-2 RBD monoclonal antibody neutralizing activity.**

301 **a,** SARS-CoV-2 pseudovirus neutralization assay. IC_{50} values for all antibodies measured at 1.3
302 months[1] and 122 selected antibodies at 6.2 months. Antibodies with IC_{50} values above 1 μg/ml
303 were plotted at 1 μg/ml. Mean of 2 independent experiments. Red bar indicates geometric mean.
304 Statistical significance was determined using two-tailed Mann-Whitney U-test. **b,** IC50 values
305 for 52 antibodies appearing at 1.3 and 6.2 months. Red bar indicates geometric mean. Statistical
306 significance was determined using two-tailed Wilcoxon matched-pairs signed rank test. **c,** IC_{50}
307 values for 5 different pairs of mAb clonal relatives obtained after 1.3 (blue) or 6.2 months (red)
308 for neutralization of wild type and mutant SARS-CoV-2 pseudovirus. Antibody IDs of the 1.3
309 months/6.2 months mAb pairs as indicated. **d,** Graph shows the normalized relative
310 luminescence values for cell lysates of $293T_{ACE2}$ cells 48 hpi with SARS-CoV-2 pseudovirus
311 harboring wt RBD or three mutant RBDs (wt, Q493R, E484G, R346S RBD mutants are shown
312 in black, red, green and blue, respectively) in the presence of increasing concentrations of two
313 mAbs C144 (1.3 months, dashed lines) or C051 (6.2 months, solid lines). Experiments were

314 performed at least twice. **e,** Surface representation of two adjacent "down" RBDs (RBD_A and
315 RBD_B) on a spike trimer with the C144 epitope on the RBDs highlighted in cyan and positions of
316 amino acid mutations that accumulated in C051 compared to the parent antibody C144
317 highlighted as stick side chains on a Cα atom representation C051 V_HV_L binding to adjacent
318 RBDs. The C051 interaction with two RBDs was modeled based on a cryo-EM structure of C144
319 Fab bound to spike trimer [17].

320 **Fig. 5: Immunofluorescence imaging of intestinal biopsies.**

321 **a,** Immunofluorescence images of human enterocytes stained for EPCAM (red), DAPI (blue) and
322 either ACE2 (green, **a** and **c**) or SARS-CoV-2 N (green, **b** and **d**) in intestinal biopsies taken 92
323 days after COVID-19 symptom onset of participant CGI-088 in the terminal ileum (**a-b**) or
324 duodenum (**c-d**). Arrows indicate enterocytes with detectable SARS-CoV-2 antigen. White scale
325 bar corresponds to 100 μm. The experiments were repeated independently at least twice with
326 similar results.

327

328

329 **Methods**
330

331 **Data reporting**

332 No statistical methods were used to predetermine sample size. The experiments were not
333 randomized and the investigators were not blinded to allocation during experiments and outcome
334 assessment.

335

336 **Study participants**. Previously enrolled study participants [1] were asked to return for a 6-month
337 follow-up visit at the Rockefeller University Hospital in New York from August 31 through
338 October 16, 2020. Eligible participants were adults aged 18-76 years and were either diagnosed
339 with SARS-CoV-2 infection by RT-PCR (cases), or were close contacts (e.g., household, co-
340 workers, members of same religious community) with someone who had been diagnosed with
341 SARS-CoV-2 infection by RT-PCR (contacts). Close contacts without seroconversion against
342 SARS-CoV-2 as assessed by serological assays (described below) were not included in the
343 subsequent analysis. Most study participants were residents of the Greater New York City tri-
344 state region and were asked to return approximately 6 months after the time of onset of COVID-
345 19 symptoms. Participants presented to the Rockefeller University Hospital for blood sample
346 collection and were asked to recall the symptoms and severity of clinical presentation during the
347 acute (first 6 weeks) and the convalescent (7 weeks until second study visit) phase of COVID-19,
348 respectively. The severity of acute infection was assessed by the WHO Ordinal Clinical
349 Progression/Improvement Scale (https://www.who.int/publications/i/item/covid-19-therapeutic-
350 trial-synopsis). Shortness of breath was assessed through the modified Medical Research Council
351 (mMRC) dyspnea scale [43]. Participants who presented with persistent symptoms attributable to
352 COVID-19 were identified on the basis of chronic shortness of breath or fatigue, deficit in

353 athletic ability and/or three or more additional long-term symptoms such as persistent
354 unexplained fevers, chest pain, new-onset cardiac sequalae, arthralgias, impairment of
355 concentration/mental acuity, impairment of sense of smell/taste, neuropathy or cutaneous
356 findings [2,3]. All participants at Rockefeller University provided written informed consent before
357 participation in the study and the study was conducted in accordance with Good Clinical
358 Practice. Clinical data collection and management were carried out using the software iRIS by
359 iMedRIS. The study was performed in compliance with all relevant ethical regulations and the
360 protocol for studies with human participants was approved by the Institutional Review Board of
361 the Rockefeller University.
362
363 **Gastrointestinal biopsy cohort.** To determine if SARS-CoV-2 can persist in the
364 gastrointestinal tract, we recruited a cohort of 14 individuals with prior diagnosis of and recovery
365 from COVID-19 illness. Eligible participants included adults, 18-76 years of age who were
366 previously diagnosed with SARS-CoV-2 by RT-PCR or through a combination of clinical
367 symptoms consistent with COVID-19 plus evidence of seroconversion, and presented to the
368 gastroenterology clinics of Mount Sinai Hospital. Endoscopic procedures were performed for
369 clinically indicated conditions as detailed in Supplementary Table 7. All participants were
370 asymptomatic at the time of the endoscopic procedures and negative for SARS-CoV-2 by nasal
371 swab PCR (Cycle threshold (Ct) cut-off <38).
372 The CLIA certified laboratory of the Mount Sinai Health System validated the laboratory-
373 developed nasopharyngeal swab real time RT-PCR test according to the New York State
374 Department of Health Wadsworth Center validation procedure for SARS-CoV-2[44]. Informed
375 consent was obtained from all participants. The biopsy-related studies were approved by the

376 Mount Sinai Ethics Committee/IRB (IRB 16-0583, The impact of viral infections and their
377 treatment on gastrointestinal immune cells).
378
379 **SARS-CoV-2 saliva PCR test**
380 The SARS-CoV-2 PCR method for saliva samples was developed and its performance
381 characteristics determined by the Rockefeller University Clinical Genomics Laboratory. This
382 laboratory-developed test has been authorized by New York State under an Emergency Use
383 Authorization (EUA) for use by authorized laboratories. Saliva was collected into guanidine
384 thiocyanate buffer as described [45]. RNA was extracted using either a column-based (Qiagen
385 QIAmp DSP Viral RNA Mini Kit, Cat#61904) or a magnetic bead-based method as described [46].
386 Reverse transcribed cDNA was amplified using primers and probes validated by the CDC or by
387 Columbia University Personalized Medicine Genomics Laboratory, respectively, and approved
388 by the FDA under the Emergency Use Authorization. Viral RNA was considered detected if the
389 cycle threshold (Ct) for two viral primers/probes were <40.
390
391 **Blood samples processing and storage.** Peripheral Blood Mononuclear Cells (PBMCs) were
392 obtained by gradient centrifugation and stored in liquid nitrogen in the presence of FCS and
393 DMSO. Heparinized plasma and serum samples were aliquoted and stored at -20°C or less. Prior
394 to experiments, aliquots of plasma samples were heat-inactivated (56°C for 1 hour) and then
395 stored at 4°C.
396
397 **High throughput automated serology assays**

398 Plasma samples from 80 out of 87 participants were tested by high throughput automated
399 serology assays. The Roche Elecsys anti-SARS-CoV-2 assay was performed on Roche Cobas
400 e411 (Roche Diagnostics, Indianapolis, IN). The Elecsys anti□SARS□CoV-2 assay uses a
401 recombinant protein representing the N antigen for the determination of antibodies against
402 SARS□CoV□2. This assay received Emergency Use Authorization (EUA) approval from the
403 United States Food and Drug Administration (FDA) [5]. The Pylon COVID-19 IgG and IgM
404 assays were used to measure plasma IgG and IgM antibodies against SARS-CoV-2, respectively.
405 Plasma samples were assayed on the Pylon 3D analyzer (ET HealthCare, Palo Alto, CA) as
406 previously described [4]. This assay was implemented clinically as a laboratory-developed test
407 under New York State Department of Health regulations. Briefly, the assay was performed using
408 a unitized test strip containing wells with pre-dispensed reagents. The COVID-19 reagent
409 contains biotinylated recombinant versions of the SARS-CoV-2 S-Protein RBD and trace
410 amounts of N protein as antigens that bind IgG and IgM, respectively. The cut off values for both
411 Pylon assays were determined using the mean of non-COVID-19 samples plus 6 Standard
412 Deviations (SDs). The results of a sample are reported in the form of a cutoff index (COI) or an
413 index value (IV), which were determined by the instrument readout of the test sample divided by
414 instrument readout at cut off.
415
416 **ELISAs**
417 ELISAs [47,48] to evaluate antibodies binding to SARS-CoV-2 N (Sino Biological 40588-V08B),
418 RBD and additional RBDs were performed by coating of high-binding 96-half-well plates
419 (Corning 3690) with 50 µl per well of a 1µg/ml protein solution in PBS overnight at 4 °C. Plates
420 were washed 6 times with washing buffer (1× PBS with 0.05% Tween-20 (Sigma-Aldrich)) and

421 incubated with 170 µl per well blocking buffer (1× PBS with 2% BSA and 0.05% Tween-20
422 (Sigma)) for 1 h at room temperature. Immediately after blocking, monoclonal antibodies or
423 plasma samples were added in PBS and incubated for 1 h at room temperature. Plasma samples
424 were assayed at a 1:67 starting dilution and 7 additional threefold serial dilutions. Monoclonal
425 antibodies were tested at 10 µg/ml starting concentration and 10 additional fourfold serial
426 dilutions. Plates were washed 6 times with washing buffer and then incubated with anti-human
427 IgG, IgM or IgA secondary antibody conjugated to horseradish peroxidase (HRP) (Jackson
428 Immuno Research 109-036-088 109-035-129 and Sigma A0295) in blocking buffer at a 1:5,000
429 dilution (IgM and IgG) or 1:3,000 dilution (IgA). Plates were developed by addition of the HRP
430 substrate, TMB (ThermoFisher) for 10 min (plasma samples) or 4 minutes (monoclonal
431 antibodies), then the developing reaction was stopped by adding 50 µl 1 M H_2SO_4 and
432 absorbance was measured at 450 nm with an ELISA microplate reader (FluoStar Omega, BMG
433 Labtech) with Omega and Omega MARS software for analysis. For plasma samples, a positive
434 control (plasma from participant COV72, diluted 66.6-fold and seven additional threefold serial
435 dilutions in PBS) was added to every assay plate for validation. The average of its signal was
436 used for normalization of all of the other values on the same plate with Excel software before
437 calculating the area under the curve using Prism V8.4 (GraphPad). For monoclonal antibodies,
438 the EC50 was determined using four-parameter nonlinear regression (GraphPad Prism V8.4).
439

440 **Expression of RBD proteins**

441 Mammalian expression vectors encoding the RBDs of SARS-CoV-2 (GenBank MN985325.1; S
442 protein residues 319-539) and eight additional mutant RBD proteins (E484K, Q493R, R346S,

443 N493K, N440K, V367F, A475V, S477N and V483A) with an N-terminal human IL-2 or Mu
444 phosphatase signal peptide were previously described [49].
445
446 **SARS-CoV-2 pseudotyped reporter virus**
447 SARS-CoV-2 pseudotyped particles were generated as previously described [1,50]. Briefly, 293T
448 cells were transfected with pNL4-3ΔEnv-nanoluc and pSARS-CoV-2-$S_{\Delta 19}$. For generation of
449 RBD-mutant pseudoviruses, pSARS-CoV-2-$S_{\Delta 19}$ carrying either of the following spike
450 mutations was used instead of its wt counterpart: Q493R, R346S or E484G [51]. Particles were
451 harvested 48 hpt, filtered and stored at -80°C.
452
453 **Pseudotyped virus neutralization assay**
454 Fourfold serially diluted plasma from COVID-19-convalescent individuals or monoclonal
455 antibodies were incubated with SARS-CoV-2 pseudotyped virus for 1 h at 37 °C. The mixture
456 was subsequently incubated with $293T_{Ace2}$ cells for 48 h after which cells were washed with PBS
457 and lysed with Luciferase Cell Culture Lysis 5× reagent (Promega). Nanoluc Luciferase activity
458 in lysates was measured using the Nano-Glo Luciferase Assay System (Promega) with the
459 Glomax Navigator (Promega). The obtained relative luminescence units were normalized to
460 those derived from cells infected with SARS-CoV-2 pseudotyped virus in the absence of plasma
461 or monoclonal antibodies. The half-maximal inhibitory concentration for plasma (NT_{50}) or
462 monoclonal antibodies (IC_{50}) was determined using four-parameter nonlinear regression (least
463 squares regression method without weighting; constraints: top=1, bottom=0) (GraphPad Prism).
464
465 **High-dimensional data analysis of flow cytometry data**

466 viSNE and FlowSOM analyses were performed on B cells using the Cytobank platform
467 (https://cytobank.org). viSNE analysis was performed using equal sampling of 4893 cells from
468 each FCS file, with 7500 iterations, a perplexity of 30, and a theta of 0.5. The following markers
469 were used to generate viSNE maps: IgA, CD305, TGFb-RII, CD138, CD10, CD272, IgD, CD24,
470 CD21, CD95, HLA-DR, IgG, CD279, CD38, IgM, CD274, CD27, CD23, CXCR5, CD32,
471 CD86, CD40, CD85j, CD11c, and CXCR3. Resulting viSNE maps were fed into the FlowSOM
472 clustering algorithm[52]. The self-organizing map (SOM) was generated using hierarchical
473 consensus clustering on the tSNE axes.
474
475 **Heatmap visualization**
476 Heatmaps to display column-scaled z-scores of MFI for individual FlowSOM clusters according
477 to marker expression were created using the R function pheatmap.
478
479 **Biotinylation of viral protein for use in flow cytometry**
480 Purified and Avi-tagged SARS-CoV-2 RBD was biotinylated using the Biotin-Protein Ligase-
481 BIRA kit according to manufacturer's instructions (Avidity) as described before [1]. Ovalbumin
482 (Sigma, A5503-1G) was biotinylated using the EZ-Link Sulfo-NHS-LC-Biotinylation kit
483 according to the manufacturer's instructions (Thermo Scientific). Biotinylated ovalbumin was
484 conjugated to streptavidin-BV711 (BD biosciences, 563262) and RBD to streptavidin-PE (BD
485 Biosciences, 554061) and streptavidin-AF647 (Biolegend, 405237)[1].
486
487 **Single-cell sorting by flow cytometry**

488 Single-cell sorting by flow cytometry was described previously [1]. Briefly, peripheral blood
489 mononuclear cells were enriched for B cells by negative selection using a pan-B-cell isolation kit
490 according to the manufacturer's instructions (Miltenyi Biotec, 130-101-638). The enriched B
491 cells were incubated in FACS buffer (1× PBS, 2% FCS, 1 mM EDTA) with the following anti-
492 human antibodies (all at 1:200 dilution): anti-CD20-PECy7 (BD Biosciences, 335793), anti-
493 CD3-APC-eFluro 780 (Invitrogen, 47-0037-41), anti-CD8-APC-eFluor 780 (Invitrogen, 47-
494 0086-42), anti-CD16-APC-eFluor 780 (Invitrogen, 47-0168-41), anti-CD14-APC-eFluor 780
495 (Invitrogen, 47-0149-42), as well as Zombie NIR (BioLegend, 423105) and fluorophore-labelled
496 RBD and ovalbumin (Ova) for 30 min on ice. Single
497 CD3−CD8−CD14−CD16−CD20+Ova−RBD-PE+RBD-AF647+ B cells were sorted into
498 individual wells of 96-well plates containing 4 µl of lysis buffer (0.5× PBS, 10 mM DTT, 3,000
499 units/ml RNasin Ribonuclease Inhibitors (Promega, N2615) per well using a FACS Aria III and
500 FACSDiva software (Becton Dickinson) for acquisition and FlowJo for analysis. The sorted cells
501 were frozen on dry ice, and then stored at −80 °C or immediately used for subsequent RNA
502 reverse transcription.
503
504 **Antibody sequencing, cloning and expression**
505 Antibodies were identified and sequenced as described previously [1]. In brief, RNA from single
506 cells was reverse-transcribed (SuperScript III Reverse Transcriptase, Invitrogen, 18080-044) and
507 the cDNA stored at −20 °C or used for subsequent amplification of the variable IGH, IGL and
508 IGK genes by nested PCR and Sanger sequencing. Sequence analysis was performed using
509 MacVector. Amplicons from the first PCR reaction were used as templates for sequence- and

510 ligation-independent cloning into antibody expression vectors. Recombinant monoclonal
511 antibodies and Fabs were produced and purified as previously described [1].
512
513 **Computational analyses of antibody sequences**
514 Antibody sequences were trimmed based on quality and annotated using Igblastn v.1.14. with
515 IMGT domain delineation system. Annotation was performed systematically using Change-O
516 toolkit v.0.4.540 [53]. Heavy and light chains derived from the same cell were paired, and
517 clonotypes were assigned based on their V and J genes using in-house R and Perl scripts
518 (Extended data Fig. 5). All scripts and the data used to process antibody sequences are publicly
519 available on GitHub (https://github.com/stratust/igpipeline).
520
521 The frequency distributions of human V genes in anti-SARS-CoV-2 antibodies from this study
522 was compared to 131,284,220 IgH and IgL sequences generated by [54] and downloaded from
523 cAb-Rep[55], a database of human shared BCR clonotypes available at https://cab-
524 rep.c2b2.columbia.edu/. Based on the 82 distinct V genes that make up the 1703 analyzed
525 sequences from Ig repertoire of the three participants present in this study, we selected the IgH
526 and IgL sequences from the database that are partially coded by the same V genes and counted
527 them according to the constant region. The frequencies shown in (Fig. S4) are relative to the
528 source and isotype analyzed. We used the two-sided binomial test to check whether the number
529 of sequences belonging to a specific IgHV or IgLV gene in the repertoire is different according
530 to the frequency of the same IgV gene in the database. Adjusted p-values were calculated using
531 the false discovery rate (FDR) correction. Significant differences are denoted with stars.
532

533 Nucleotide somatic hypermutation and CDR3 length were determined using in-house R and Perl
534 scripts. For somatic hypermutations, IGHV and IGLV nucleotide sequences were aligned against
535 their closest germlines using Igblastn and the number of differences were considered nucleotide
536 mutations. The average mutations for V genes was calculated by dividing the sum of all
537 nucleotide mutations across all participants by the number of sequences used for the analysis. To
538 calculate the GRAVY scores of hydrophobicity [56] we used Guy H.R. Hydrophobicity scale based
539 on free energy of transfer (kcal/mole) [57] implemented by the R package Peptides (the
540 Comprehensive R Archive Network repository; https://journal.r-project.org/archive/2015/RJ-
541 2015-001/RJ-2015-001.pdf). We used 532 heavy chain CDR3 amino acid sequences from this
542 study and 22,654,256 IGH CDR3 sequences from the public database of memory B cell receptor
543 sequences [58]. The Shapiro–Wilk test was used to determine whether the GRAVY scores are
544 normally distributed. The GRAVY scores from all 532 IGH CDR3 amino acid sequences from
545 this study were used to perform the test and 5,000 GRAVY scores of the sequences from the
546 public database were randomly selected. The Shapiro–Wilk P values were 6.896×10^{-3} and
547 2.217×10^{-6} for sequences from this study and the public database, respectively, indicating that
548 the data were not normally distributed. Therefore, we used the two-tailed Wilcoxon
549 nonparametric test to compare the samples, which indicated a difference in hydrophobicity
550 distribution ($P = 5 \times 10^{-6}$) (Extended data Fig. 6h).
551
552 Heatmap of log2 relative fold change in EC50 against the indicated RBD mutants for antibody
553 clonal pairs obtained at 1.3 and 6.2 months (Fig.3e and Extended data Fig. 7k) was created with
554 R pheatmap package (https://github.com/raivokolde/pheatmap) using Euclidean distance and
555 Ward.2 clustering method.

556

557 **Biopsies and Immunofluorescence**

558 Endoscopically obtained mucosal biopsies were formalin fixed and paraffin embedded. Sections
559 (5µm) were cut, dewaxed in xylene, and rehydrated in graded alcohol and phosphate-buffered
560 saline (PBS). Heat-induced epitope retrieval was performed in target retrieval solution (Dako,
561 S1699) using a commercial pressure cooker. Slides were then cooled to room temperature,
562 washed in PBS and permeabilized for 30 minutes in 0.1% Triton X-100 in PBS. Non-specific
563 binding was blocked with 10% goat serum (Invitrogen, 50062Z) for 1 hour at room temperature.
564 Sections were then incubated with a combination of primary antibodies diluted in blocking
565 solution overnight at 4°C. Slides were washed 3 times in PBS and then incubated in secondary
566 antibody and 4′,6-diamidino-2-phenylindole (1ug/mL) for 1 hour at room temperature. Sections
567 were washed in PBS 3 times and then mounted with Fluoromount-G (Electron Microscopy
568 Sciences, 1798425). Controls included, omitting primary antibody (no primary 995 control), or
569 substituting primary antibodies with non-reactive antibodies of the same isotype (isotype
570 control). A Nikon Eclipse Ni microscope and digital SLR camera (Nikon, DS-Qi2) was used to
571 visualize and image the tissue.

572

573 The antibody used to stain sections for N protein was raised in rabbits against SARS-CoV N and
574 is cross-reactive with SARS-CoV-2 N protein [59].

575

Antigen	Clone	Vendor	Catalogue number	Host species	Conjugate	Dilution
ACE2	Polyclonal	Abcam	ab15348	rabbit	unconjugated	1:1000

EPCAM	SPM491	GeneTex	GTX34693	mouse	unconjugated	1:100
SARS-CoV-2 nucleocapsid	Polyclonal	Spiegel, M. *et al.*[59]	N/A	rabbit	unconjugated	1:2000
No known specificity (isotype control)	Polyclonal	Abcam	ab37415	rabbit	unconjugated	1:100 to 1:2000 corresponding to the concentration of the targeted polyclonal rabbit antibody
Yeast GAL4 (isotype control)	15-6E10A7	Abcam	ab170190	mouse	unconjugated	1:100 to 1:2000 corresponding to the concentration of the targeted monoclonal mouse antibody
Mouse IgG H&L	Polyclonal	Abcam	ab150116	goat	Alexa Fluor 594	1:1000
Rabbit IgG H&L	Polyclonal	Abcam	ab150077	goat	Alexa Fluor 488	1:1000

576

577 **SARS-CoV-2 PCR (intestinal biopsies)**

578 To determine if SARS-CoV-2 RNA is present in the gastrointestinal tract we isolated
579 RNA from endoscopically obtained mucosal biopsies using Direct-zol miniprep kit (Zymo
580 research, Cat. No. R2050). Reverse transcribed cDNA was amplified using 2019-nCov Ruo Kit
581 (IDT) to detect viral nucleocapsid genomic RNA. Amplification of sub-genomic nucleocapsid
582 RNA was done using following primers and probe: sgLeadSARSCov2_F 5'-
583 CGATCTCTTGTAGATCTGTTCTC -3'[27], wtN_R4 5' – GGTGAACCAAGACGCAGTAT –
584 3', wtN_P4 5' – /56-FAM/TAACCAGAA/ZEN/TGGAGAACGCAGTGGG/3IABkFQ/ – 3'.

585 Quantitative PCR was performed using QuantTect probe PCR kit (Qiagen, Cat. No. 204345)
586 under following conditions: 95 15', 95°C 15 sec, 60°C 1 min using the Applied Biosystem
587 QuantStudio 6 Flex Real-Time PCR System. Viral RNA was considered detected if the cycle
588 threshold (Ct) for viral primers/probes was <40. Samples from positive wells were column
589 purified and presence of N1 sequences additionally verified by Sanger sequencing.
590
591 **SARS-CoV-2 RNA detection by probes proximity ligation.**
592 Probes were designed with a 20-25 nucleotides homology to SARS-CoV-2 genomic RNA.
593 Probes were assessed by NCBI BLAST to exclude off target binding to other cellular transcripts.
594 IDT OligoAnalyzer (Integrated DNA Technologies) was used to identify probe pairs with similar
595 thermodynamic properties; melting temperature 45-60ºC, GC content of 40-55%, and low self-
596 complementary. The 3' end of each one of the probes used for proximity ligation signal
597 amplification is designed with a partially complementary sequence to the 61bp long backbone
598 and partially to the 21bp insert as previously described (Supplementary Table 8). smFISH probes
599 were designed with a complementary 3' end to the biotin detection probe (Supplementary Table
600 8).
601
602 Paraffin embedded samples were sectioned at ten microns. Sections were deparaffinized using
603 100% xylene, 5 min at room temperature, repeated twice. Slides were rinsed in 100% ethanol, 1
604 min at room temperature, twice and air dried. Endogenous peroxidase activity was eliminated by
605 treating the samples with 0.3% hydrogen peroxide, 10 min at room temperature followed by
606 washing with DEPC treated water. Samples were incubated 15 min at 95-100 °C in antigen
607 retrieval solution (ACDBio, Newark, CA, USA) rinsed in DEPC treated water and dehydrated in

608 100% ethanol, 3 min at room temperature and air dried. Tissue sections were permeabilized 30
609 min at 40°C using RNAscope protease plus solution (ACDBio, Newark, CA, USA) and rinsed in
610 DEPC treated water.
611 Hybridization was performed overnight at 40°C in a buffer based on DEPC-treated water
612 containing 2× SSC, 20% formamide (Thermo Fischer Scientific, Waltham, MA, USA), 2.5 %
613 (vol/vol) polyvinylsulfonic acid, 20 mM ribonucleoside vanadyl complex (New England Biolabs,
614 Ipswich, MA, USA), 40 U/ml RNasin (Promega, Madison, WI, USA), 0.1% (vol/vol) Tween 20
615 (Sigma Aldrich), 100 µg/ml salmon sperm DNA (Thermo Fisher Scientific, Waltham, MA,
616 USA), 100 µg/ml yeast RNA (Thermo Fisher Scientific, Waltham, MA, USA). DNA probes
617 dissolved in DEPC-treated water were added at a final concentration of 100nM (Integrated DNA
618 Technologies, Coralville, IA, ISA). Samples were washed briefly and incubated in a buffer
619 containing, 2× SSC, 20% formamide, 40 U/ml RNasin at 40 °C and then washed four times (5
620 min each) in wash buffer, PBS, 0.1% (vol/vol) Tween 20, and 4 U/ml RNasin (Promega,
621 Madison, WI, USA). Slides were then incubated with 100 nM insert/backbone oligonucleotides
622 in PBS, 1× SSC, 0.1% (vol/vol) Tween 20, 100 µg/ml salmon sperm DNA (Thermo Fisher
623 Scientific, Waltham, MA, USA), 100 µg/ml yeast RNA (Thermo Fisher Scientific, Waltham,
624 MA, USA), 40 U/ml RNasin at 37 °C. After four washes, tissues were incubated at 37°C with
625 0.1 U/µl T4 DNA ligase (New England Biolabs, Ipswich, MA, USA) in 50mM Tris-HCl, 10mM
626 MgCl2, 1mM ATP, 1mM DTT, 250µg/ml BSA, 0.05% Tween 20, 40 U/ml RNasin, followed by
627 incubation with 0.1 U/µl phi29 DNA polymerase in 50 mM Tris–HCl, 10 mM MgCl2, 10 mM
628 (NH4)2SO4, 250□M dNTPs, 1mM DTT, 0.05% Tween 20, 40 U/ml RNasin pH 7.5 at 30 °C.
629 Slides were washed and endogenous biotin was blocked using Avidin/Biotin blocking kit
630 (Vector laboratories, Burlingame, CA, USA) according to the manufacture instructions. Rolling

631 cycle amplicons were identified using a biotin labeled DNA probe at a concentration of 5 nM at
632 37 °C in PBS, 1× SSC, 0.1% Tween 20, 100 μg/ml salmon sperm DNA, 100 μg/ml yeast RNA.
633 After washing, samples were incubated with 1:100 diluted streptavidin-HRP (Thermo Fisher
634 Scientific, Waltham, MA, USA) in PBS, 60 min at room temperature followed by washing.
635 Fluorescent labeling was accomplished using Alexa Fluor 647 Tyramide SuperBoostKit (Thermo
636 Fischer Scientific, Waltham, MA, USA) according to manufacture instructions. Hoechst 33342
637 was used for nuclear counterstaining (Thermo Fischer Scientific, Waltham, MA, USA) and
638 samples were mounted in ProLong gold antifade (Thermo Fischer Scientific, Waltham, MA,
639 USA).
640
641 **SARS-CoV-2 RNA detection by smFISH.**
642 Hybridization was performed overnight at 40°C in a buffer based on DEPC- treated water
643 containing 2× SSC, 20% formamide (Thermo Fischer Scientific, Waltham, MA, USA), 2.5 %
644 (vol/vol) polyvinylsulfonic acid, 20 mM ribonucleoside vanadyl complex (New England Biolabs,
645 Ipswich, MA, USA), 40 U/ml RNasin (Promega, Madison, WI, USA), 0.1% (vol/vol) Tween 20
646 (Sigma Aldrich), 100 μg/ml salmon sperm DNA (Thermo Fisher Scientific, Waltham, MA,
647 USA), 100 μg/ml yeast RNA (Thermo Fisher Scientific, Waltham, MA, USA). DNA probes
648 dissolved in DEPC-treated water were added at a final concentration of 10nM (Integrated DNA
649 Technologies, Coralville, IA, ISA). Samples were washed briefly and incubated in a buffer
650 containing, 2× SSC, 20% formamide, 40 U/ml RNasin at 40 °C and then washed four times in
651 wash buffer, PBS, 0.1% (vol/vol) Tween 20, and 4 U/ml RNasin (Promega, Madison, WI, USA).
652 Samples were washed and endogenous biotin was blocked using Avidin/Biotin blocking kit
653 (Vector laboratories, Burlingame, CA, USA) according to the manufacture instructions. Slides

654 were incubated with a biotin labeled DNA probe at a concentration of 10 nM at 37 °C in PBS, 1×
655 SSC, 0.1% Tween 20, 100 μg/ml salmon sperm DNA, 100 μg/ml yeast RNA. After washing,
656 samples were incubated with 1:100 diluted streptavidin-HRP (Thermo Fisher Scientific,
657 Waltham, MA, USA) in PBS, 60 min at room temperature followed by washing. Samples were
658 labeled using ImmPACT-DAB substrate, counter stained using hematoxylin QS and imbedded in
659 VectaMount AQ mounting medium (Vector laboratories, Burlingame, CA, USA) according to
660 the manufacture instructions.
661
662 **Data presentation**
663 Figures arranged in Adobe Illustrator 2020.
664
665
666 **Competing interests:** The Rockefeller University has filed a provisional patent application in
667 connection with this work on which D.F.R. and M.C.N. are inventors (US patent 63/021,387).
668 R.E.S. is on the scientific advisory board of Miromatrix Inc and is a consultant and speaker for
669 Alnylam Inc. S.M. has served as a consultant for Takeda Pharmaceuticals, Morphic and Glaxo
670 Smith Kline. Z.Z. received seed instruments and sponsored travel from ET Healthcare.
671
672 **Data availability statement:** Data are provided in SI Tables 1-8. The raw sequencing data and
673 computer scripts associated with Figure 2 have been deposited at Github
674 (https://github.com/stratust/igpipeline). This study also uses data from "A Public Database of
675 Memory and Naive B-Cell Receptor Sequences" (https://doi.org/10.5061/dryad.35ks2), PDB

676 (6VYB and 6NB6) and from "High frequency of shared clonotypes in human B cell receptor
677 repertoires" (https://doi.org/10.1038/s41586-019-0934-8).
678
679 **Code availability statement:** Computer code to process the antibody sequences is available at
680 GitHub (https://github.com/stratust/igpipeline).
681
682 **Acknowledgements:** We thank all study participants who devoted time to our research; Drs.
683 Barry Coller and Sarah Schlesinger, the Rockefeller University Hospital Clinical Research
684 Support Office and nursing staff. Mayu Okawa Frank and Robert B. Darnell for SARS-CoV-2
685 saliva PCR testing. Charles M. Rice and all members of the M.C.N. laboratory for helpful
686 discussions and Maša Jankovic for laboratory support. This work was supported by NIH grant
687 P01-AI138398-S1 (M.C.N. and P.J.B.) and 2U19AI111825 (M.C.N.).; the Caltech Merkin
688 Institute for Translational Research and P50 AI150464-13 (P.J.B.), George Mason University
689 Fast Grant (D.F.R. and P.J.B.) and the European ATAC consortium EC 101003650 (D.F.R.);
690 R37-AI64003 to P.D.B.; R01AI78788 to T.H.; NCI R01CA234614, NIAID 2R01AI107301,
691 NIDDK R01DK121072 and 1RO3DK117252 to R.E.S., NIH NIDDK R01 DK123749 01S1 to
692 S.M. We thank Dr. Jost Vielmetter and the Protein Expression Center in the Beckman Institute at
693 Caltech for expression assistance. C.O.B. is supported by the HHMI Hanna Gray and Burroughs
694 Wellcome PDEP fellowships. R.E.S. is a Irma Hirschl Trust Research Award Scholar. M.T. is
695 supported by the Digestive Disease Research Foundation (DDRF). C.G. was supported by the
696 Robert S. Wennett Post-Doctoral Fellowship, in part by the National Center for Advancing
697 Translational Sciences (National Institutes of Health Clinical and Translational Science Award

698 program, grant UL1 TR001866), and by the Shapiro-Silverberg Fund for the Advancement of
699 Translational Research. P.D.B. and M.C.N. are Howard Hughes Medical Institute Investigators.
700
701 **Author Contributions:** C.G., P.D.B., P.J.B., T.H., S.M. and M.C.N. conceived, designed and
702 analyzed the experiments. D.F.R., M.Caskey. and C.G. designed clinical protocols. Z.W.,
703 J.C.C.L., F.M., S.F., M.T., A.C., M.J., D.S.B., F.S., Y.W., T.H., P.M., G.B., C.V., C.O.B., K.G.,
704 D.J., J.Y., G.M.D., Y.B., R.E.S. and Z.Z. carried out experiments. A.G. and M.Cipolla produced
705 antibodies. A.H., D.S.B., M.Turroja, K.G.M., M.Tankelevich, C.G. and M.Caskey recruited
706 participants and executed clinical protocols. I.S., R.P, J.D. and C.U.O. processed clinical
707 samples. T.Y.O. and V.R. performed bioinformatic analysis. C.G, P.D.B., P.J.B., T.H., S.M. and
708 M.C.N. wrote the manuscript with input from all co-authors.
709

710 **Extended Data Legends**

711 **Extended Data Fig. 1: Clinical correlates of plasma antibody titres.**
712 **a**, Normalized AUC anti-RBD IgG titres at 1.3 months for participants with (n=38) or without
713 (n=49) persistent post-acute symptoms. **b**, Normalized AUC anti-RBD IgG titres at 6.2 months
714 for participants with (n=38) or without (n=49) persistent post-acute symptoms. **c**, Normalized
715 AUC anti-RBD IgM titres at 1.3 months for participants with (n=38) or without (n=49) persistent
716 post-acute symptoms. **d**, Normalized AUC anti-RBD IgM titres at 6.2 months for participants
717 with (n=38) or without (n=49) persistent post-acute symptoms. **e**, Normalized AUC anti-RBD
718 IgA titres at 1.3 months for participants with (n=38) or without (n=49) persistent post-acute
719 symptoms. **f**, Normalized AUC anti-RBD IgA titres at 6.2 months for participants with (n=38) or
720 without (n=49) persistent post-acute symptoms. **g**, Normalized AUC anti-N IgG titres at 1.3
721 months for participants with (n=38) or without (n=49) persistent post-acute symptoms. **h**,
722 Normalized AUC anti-N IgG titres at 6.2 months for participants with (n=38) or without (n=49)
723 persistent post-acute symptoms. **i**, IV values of anti-RBD IgG titres at 1.3 months for participants
724 with (n=38) or without (n=49) persistent post-acute symptoms. **j**, IV values of anti-RBD IgG
725 titres at 6.2 months for participants with (n=38) or without (n=49) persistent post-acute
726 symptoms. **k**, COI values of anti-N total Ig titres at 1.3 months for participants with (n=38) or
727 without (n=49) persistent post-acute symptoms. **l**, COI values of anti-N total Ig titres at 6.2
728 months for participants with (n=38) or without (n=49) persistent post-acute symptoms. **m**, NT50
729 values at 1.3 months for participants with (n=38) or without (n=49) persistent post-acute
730 symptoms. **n**, NT50 values at 6.2 months for participants with (n=38) or without (n=49)
731 persistent post-acute symptoms. **o**, Age in years for participants with (n=38) or without (n=49)
732 persistent post-acute symptoms. **p**, Severity of acute infection as assessed by the WHO Ordinal

733 Clinical Progression/Improvement Scale for participants with (n=38) or without (n=49)
734 persistent post-acute symptoms. **q**, Duration of Symptoms during acute infection for participants
735 with (n=38) or without (n=49) persistent post-acute symptoms. Horizontal bars indicate median
736 values. Statistical significance was determined using two-tailed Mann–Whitney U-tests.

737

738 **Extended Data Fig. 2: Correlations of plasma antibody measurements.**

739 **a,** Normalized AUC for IgG anti-RBD plotted against Pylon IgG anti-RBD index values at 1.3
740 months. **b,** Normalized AUC for IgG anti-RBD plotted against Pylon IgG anti-RBD index values
741 at 6.2 months. **c,** Normalized AUC for IgM anti-RBD plotted against Pylon IgM anti-RBD index
742 values at 1.3 months. **d,** Normalized AUC for IgM anti-RBD plotted against Pylon IgM anti-
743 RBD index values at 6.2 months. **e**, Normalized AUC for IgG anti-N plotted against Roche COI
744 values for anti-N total Ig titres at 1.3 months. **f,** Normalized AUC for IgG anti-N plotted against
745 Roche COI values for anti-N total Ig titres at 6.2 months. **g**, Anti-N total Ig Cut-off Index (COI)
746 values for 80 individuals at the initial 1.3 and 6.2 month follow-up visit. **h**, Relative change in
747 anti-N total Ig levels between 1.3 and 6.2 months plotted against the anti-N total Ig levels at 1.3
748 months. **i,** Normalized AUC for IgM anti-RBD at 6.2 months plotted against IgM anti-RBD at
749 1.3 months. **j**, Normalized AUC for IgG anti-RBD at 6.2 months plotted against IgG anti-RBD at
750 1.3 months. **k**, Normalized AUC for IgA anti-RBD at 6.2 months plotted against IgA anti-RBD
751 at 1.3 months. **l**, Normalized AUC for IgG anti-N at 6.2 months plotted against IgG anti-N at 1.3
752 months. **m**, COI values for anti-N total Ig titres at 6.2 months plotted against anti-N total Ig titres
753 at 1.3 months. **n**, Anti-RBD IgM titres at 1.3 months plotted against anti-N IgG titres at 1.3
754 months. **o,** Anti-RBD IgG titres at 1.3 months plotted against anti-N IgG titres at 1.3 months. **p,**

755 Anti-RBD IgA titres at 1.3 months plotted against anti-N IgG titres at 1.3 months. **q**, NT50
756 values at 1.3 months plotted against anti-RBD IgG titres at 1.3 months. **r**, NT50 values at 6.2
757 months plotted against anti-RBD IgG titres at 6.2 months. The *r* and *p* values were determined
758 by two-tailed Spearman's correlations.

759

760 **Extended Data Fig. 3: Persistent longitudinal changes in the phenotypic landscape of B**
761 **cells in individuals recovered from COVID-19**

762 **a**, Global viSNE projection of pooled B cells for all participants pooled shown in background
763 contour plots, with overlaid projections of concatenated controls, convalescent participants 1.3
764 and 6.1 months respectively. **b**, viSNE projection of pooled B cells for all participants of B cell
765 clusters identified by FlowSOM clustering. Column-scaled z-scores of median fluorescence
766 intensity (MFI) as indicated by cluster and marker. **c**, Frequency of B cells from each group in
767 FlowSOM clusters indicated. Each circle represents an individual control individual (n=20)
768 (gray), convalescent participant at 1.3 months post-infection (n=41) (red), or convalescent
769 participant at 6.2 months post-infection (n=41) (green). Horizontal bars indicate mean values.
770 Significance determined by two-tailed paired t-test for comparisons between time points within
771 individuals and two-tailed unpaired t-test for comparison between controls and convalescent
772 individuals. **d**, Individual viSNE projections of indicated protein expression.

773

774 **Extended Data Fig. 4: Flow cytometry.**

775 **a,** Gating strategy used for cell sorting. Gating was on singlets that were CD20+ and
776 CD3−CD8−CD16−Ova−. Sorted cells were RBD-PE+ and RBD-AF647+. **b,** Flow cytometry
777 showing the percentage of RBD-double positive memory B cells from month 1.3 or month 6
778 post-infection in 21 randomly selected participants.

779

780 **Extended Data Fig. 5: Frequency distributions of human V genes.**
781 **a,** Two-sided binomial tests were used to compare the frequency distributions of human V genes
782 of anti-SARS-CoV-2 antibodies from donors at 1.3 months to 6.2 months [1] (* $p < 0.05$, ** $p <$
783 0.01
784 *** $p < 0.001$, **** = $p < 0.0001$). **b,** Two-sided binomial tests were used to compare the
785 frequency distributions of human V genes of anti-SARS-CoV-2 antibodies from this study to
786 sequence from *C. Soto et al.* [54] (* $p < 0.05$, ** $p < 0.01$, *** $p < 0.001$, **** = $p < 0.0001$). **c**,
787 Sequences from all six individuals with clonal relationships depicted as circos plots as in Figure
788 2d. Interconnecting lines indicate the relationship between antibodies that share V and J gene
789 segment sequences at both IGH and IGL. Purple, green and grey lines connect related clones,
790 clones and singles, and singles to each other, respectively. **d,** For each participant, the number of
791 IgG heavy chain sequences (black) analyzed at month 1.3 (left panel) or month 6.2 post-infection
792 (right panel). The number in the inner circle indicates the number of cells that was sorted for
793 each individual denoted above the circle. **e,** The same as d but showing combined data for all six
794 participants. **f,** Comparison of the percentage of IgG positive B cells from all six individuals at
795 month 1.3 or month 6.2 post-infection. The horizontal bars indicate the mean. Statistical
796 significance was determined using two-tailed t-test.

797

798 **Extended Data Fig. 6: Analysis of antibody somatic hypermutation of persisting clones,**
799 **CDR3 length and hydrophobicity.**

800 **a-f**, Number of somatic nucleotide mutations in both the IGVH and IGVL of persisting clones
801 found at month 1.3 and month 6.2 time points in six participants (a) COV21, (b) COV47, (c)
802 COV57, (d) COV72, (e) COV96, and (f) COV107. The VH and VL gene usage of each clonal
803 expansion is indicated above the graphs, or are indicated as "Singlets" if the persisting sequence
804 was isolated only once at both time points. Connecting line indicates the SHM of the clonal pairs
805 that were expressed as a recombinant mAbs. **g,** For each individual, the number of the amino
806 acid length of the CDR3s at the IGVH and IGVL is shown. The horizontal bars indicate the
807 mean. The number of antibody sequences (IGVH and IGVL) evaluated for each participant are n
808 = 90 (COV21), n = 78 (COV47), n = 53 (COV57), n = 87 (COV72), n = 104 (COV96), n = 120
809 (COV107). Right panel show all antibodies combined (n = 532 for both IGVH and IGVL).
810 Statistical significance was determined using two-tailed Mann–Whitney U-tests and horizontal
811 bars indicate median values (n.s.=non-significant, * $p < 0.05$, ** $p < 0.01$, *** $p < 0.001$, **** =
812 $p < 0.0001$). **h,** Distribution of the hydrophobicity GRAVY scores at the IGH CDR3 in 532
813 antibody sequences from this study compared to a public database (see Methods for statistical
814 analysis). The box limits are at the lower and upper quartiles, the center line indicates the
815 median, the whiskers are 1.5× interquartile range and the dots represent outliers. Statistical
816 significance was determined using two-tailed Wilcoxon matched-pairs signed rank test
817 (n.s.=non-significant, * $p < 0.05$, ** $p < 0.01$, *** $p < 0.001$, **** = $p < 0.0001$).

818

819 **Extended Data Fig. 7: ELISA of wt/mutant RBD for mAbs.**

820 **a,** EC50 values for binding to wild type RBD of shared singlets and shared clones of mAbs
821 obtained at the initial 1.3 and 6.2 months follow-up visit, divided by participant (n = 6 (COV21),
822 n = 13 (COV47), n = 3 (COV57), n = 6 (COV72), n = 15 (COV96), n = 9 (COV107). Lines
823 connect shared singlets/clones. mAbs with improved EC50 at 6.2 months follow-up visit are
824 highlighted in green, remaining mAbs are shown in black. Statistical significance was
825 determined using two-tailed Wilcoxon matched-pairs signed rank test. **b-j,** Graphs show ELISA
826 binding curves for different antibodies obtained at 1.3 months (dashed lines) and their clonal
827 relatives obtained after 6.2 months (solid lines) binding to wild type, R346S, E484K, Q493R,
828 N439K, N440K, A475V, S477N, V483A and V367F RBDs (colors as indicated). Antibody IDs
829 of pairs as indicated on top of panels (1.3m / 6.2m). **k,** Heat map shows log2 relative fold change
830 in EC_{50} against the indicated RBD mutants for 52 antibody clonal pairs obtained at 1.3 (black)
831 and 6.2 months (red). The clonal and participant origin for each antibody pair is indicated above.
832
833 **Extended Data Fig. 8: Neutralization of wt/mutant RBDs, C51 alignment and binding**
834 **projection.**
835 **a,** IC50 values of shared singlets and shared clones of mAbs obtained at the initial 1.3- and 6.2-
836 months follow-up visit, divided by participant (n = 6 (COV21), n = 13 (COV47), n = 3 (COV57),
837 n = 6 (COV72), n = 15 (COV96), n = 9 (COV107). Lines connect shared singlets/clones. mAbs
838 with undetectable IC50 at 1.3 months are plotted at 10 µg/ml and are highlighted in red, mAbs
839 with improved IC50 at 6.2 months follow-up visit are highlighted in green, remaining mAbs are
840 shown in black. Statistical significance was determined using two-tailed Wilcoxon matched-pairs
841 signed rank test. **b-f,** The normalized relative luminescence values for cell lysates of 293TAce2
842 cells 48 hpi with SARS-CoV-2 pseudovirus harboring wt RBD or RBD-mutants (wt, Q493R,

843 E484G and R346S RBD shown in black, red, green and blue, respectively) in the presence of
844 increasing concentrations of mAbs obtained at the 1.3 months initial visit (1.3m, dashed lines)
845 and their shared clones/singlets at the 6.2 follow-up visit (6.2m, continuous lines). Antibody IDs
846 as indicated. **g,** VH and VL amino acid sequence alignment of C144 and derivative antibodies
847 C051, C052, C053 and C054. Germline-encoded residues are highlighted in green. Residues in
848 the proximity of RBD-binding C144 paratope are highlighted in red.
849 **h-j**, Surface representation of two adjacent "down" RBDs (RBD_A and RBD_B) on a spike trimer
850 with the C144 epitope on the RBDs highlighted in cyan and positions of amino acid mutations
851 that accumulated in **h,** C052. **i**, C053 and **j**, C054 compared to the parent antibody C144
852 highlighted as stick side chains on a Cα atom representation. The C052, C053 and C054
853 interactions with two RBDs was modeled based on a cryo-EM structure of C144 Fab bound to
854 spike trimer [17].
855
856 **Extended Data Fig. 9**: **SARS-CoV-2 antigen in human enterocytes in the gastrointestinal**
857 **tract 3 months post COVID-19 and Pre-COVID-19 historic control individuals without**
858 **detectable SARS-CoV-2 antigen.**
859 **a-j**, Immunofluorescence images of human gastrointestinal tissue are shown. Staining is for
860 EPCAM (red), DAPI (blue) and SARS-CoV-2 nucleocapsid (green) Samples are derived from
861 intestinal biopsies in the gastrointestinal tract as indicated (a-j). (a-h) are biopsies from
862 participant CGI-088 (Supplementary Table 7) taken 92 days post COVID-19 symptom onset. (i-
863 j) is a biopsy 27 months prior to COVID-19 symptom onset from the same participant CGI-088.
864 Arrows indicate enterocytes with detectable SARS-CoV-2 antigen. Isotype and no primary
865 controls for each tissue are shown in the right two columns. White scale bar corresponds to 100

866 µm. **k-l**, Immunofluorescence images of biopsy samples in the gastrointestinal tract (k-ileal, l-
867 duodenal) obtained from 10 different Pre-COVID-19 historic control individuals between
868 January 2018 and October 2019 are shown. Staining is for EPCAM (red), DAPI (blue) and
869 SARS-CoV-2 nucleocapsid (green). White scale bar corresponds to 100 µm. All experiments
870 were repeated independently at least twice with similar results.
871
872 **Extended Data Fig. 10**: **SARS-CoV-2 antigen and RNA is detectable in different intestinal**
873 **segments in multiple COVID-19 convalescent individuals**
874 **a**, Immunofluorescence (IF) images of biopsy samples in the gastrointestinal tract in different
875 individuals are shown. Staining is for EPCAM (red), DAPI (blue) and SARS-CoV-2
876 nucleocapsid (green). Samples are derived from intestinal biopsies from 4 participants (CGI089,
877 CGI092, CGI100 and CGI106) taken at least 3 months after COVID-19 infection. Arrows
878 indicate enterocytes with detectable SARS-CoV-2 antigen. White scale bar corresponds to 100
879 µm. The experiments were repeated independently at least twice with similar results. **b**,
880 Quantification of SARS-CoV-2 positive cells by immunofluorescence. The number of cells
881 staining positive for the nucleocapsid protein (N) of SARS-CoV-2 per mm^2 of intestinal
882 epithelium is shown. The graphs show biopsy samples from the indicated individuals of the
883 duodenum (left) and terminal ileum (right), respectively. Black dots represent the number of
884 available biopsy specimen for each individual from the respective intestinal segment (CGI-088
885 n=4 duodenal/n=2 ileal, CGI-089 n=2 duodenal/n=2 ileal, CGI-092 n=6 duodenal/n=3 ileal,
886 CGI-106 n=4, CGI-100 n=4). Boxes represent median values and whiskers the 95 % CI. **c-d,**
887 SARS-CoV-2 viral RNA was visualized in intestinal biopsies of participant CGI-089 (c) and
888 CGI-088 (d) using in situ hybridization. SARS-CoV-2 genomic RNA (black) and Hematoxylin

889 and Eosin staining by smFISH/IHC technique in the duodenum (left) or terminal ileum (right).
890 Arrows indicate enterocytes with detectable SARS-CoV-2 RNA. **e**, Pre-COVID-19 historic
891 control individuals show no detectable SARS-CoV-2 viral RNA in duodenal (left) or ileal (right)
892 biopsies. White scale bar corresponds to 100 μm. The experiments were repeated independently
893 three times with similar results.
894

895

896 **Supplementary Tables**

897 **Supplementary Table 1: Cohort summary is provided as a separate Excel file.**

898 **Supplementary Table 2: Individual participant characteristics is provided as a separate**
899 **Excel file.**

900 **Supplementary Table 3: Antibody sequences from 1.3 and 6.2 month time point is provided**
901 **as a separate Excel file.**

902 **Supplementary Table 4: Sequences of the cloned monoclonal antibodies is provided as a**
903 **separate Excel file.**

904 **Supplementary Table 5: Half maximal effective concentrations (EC50s) of the monoclonal**
905 **antibodies is provided as a separate Excel file.**

906 **Supplementary Table 6: Inhibitory concentrations of the monoclonal antibodies is**
907 **provided as a separate Excel file.**

908 **Supplementary Table 7: Gastrointestinal biopsies cohort characteristics is provided as a**
909 **separate Excel file.**

910 **Supplementary Table 8: Proximity ligation and smFISH probe sequences is provided as a**
911 **separate Excel file.**

912

913 **References**

914 1 Robbiani, D. F. *et al*. Convergent antibody responses to SARS-CoV-2 in convalescent
915 individuals. *Nature* **584**, 437-442, doi:10.1038/s41586-020-2456-9 (2020).
916 2 Carfi, A., Bernabei, R., Landi, F. & Gemelli Against, C.-P.-A. C. S. G. Persistent
917 Symptoms in Patients After Acute COVID-19. *JAMA* **324**, 603-605,
918 doi:10.1001/jama.2020.12603 (2020).
919 3 American Medical Association. Long-term Health Consequences of COVID-19. 1-2,
920 doi:10.1001/jama.2020.20677 (2020).
921 4 Yang, H. S. *et al*. SARS-CoV-2 antibody characterization in emergency department,
922 hospitalized and convalescent patients by two semi-quantitative immunoassays. *Clin*
923 *Chim Acta* **509**, 117-125, doi:10.1016/j.cca.2020.06.004 (2020).
924 5 Roche Diagnostics. *Elecsys Anti-SARS-CoV-2*, <https://www.fda.gov/media/137605>
925 (2020).
926 6 Muecksch, F. *et al*. Longitudinal analysis of serology and neutralizing antibody levels in
927 COVID19 convalescents. *The Journal of Infectious Diseases*, doi:10.1093/infdis/jiaa659
928 (2020).
929 7 Schmidt, F. *et al*. Measuring SARS-CoV-2 neutralizing antibody activity using
930 pseudotyped and chimeric viruses. *J Exp Med* **217**, 284-218, doi:10.1084/jem.20201181
931 (2020).
932 8 Wajnberg, A. *et al*. Robust neutralizing antibodies to SARS-CoV-2 infection persist for
933 months. *Science (New York, N.Y.)*, eabd7728-7727, doi:10.1126/science.abd7728 (2020).
934 9 Seow, J. *et al*. Longitudinal observation and decline of neutralizing antibody responses in
935 the three months following SARS-CoV-2 infection in humans. *Nat Microbiol*, 1-17,
936 doi:10.1038/s41564-020-00813-8 (2020).
937 10 Brouwer, P. J. M. *et al*. Potent neutralizing antibodies from COVID-19 patients define
938 multiple targets of vulnerability. *Science (New York, N.Y.)* **369**, 643-650,
939 doi:10.1126/science.abc5902 (2020).
940 11 Cao, Y. *et al*. Potent Neutralizing Antibodies against SARS-CoV-2 Identified by High-
941 Throughput Single-Cell Sequencing of Convalescent Patients' B Cells. *Cell* **182**, 73-84
942 e16, doi:10.1016/j.cell.2020.05.025 (2020).
943 12 Ju, B. *et al*. Human neutralizing antibodies elicited by SARS-CoV-2 infection. *Nature*
944 **584**, 115-119, doi:10.1038/s41586-020-2380-z (2020).
945 13 Kreer, C. *et al*. Longitudinal Isolation of Potent Near-Germline SARS-CoV-2-
946 Neutralizing Antibodies from COVID-19 Patients. *Cell* **182**, 843-854 e812,
947 doi:10.1016/j.cell.2020.06.044 (2020).
948 14 Seydoux, E. *et al*. Analysis of a SARS-CoV-2-Infected Individual Reveals Development
949 of Potent Neutralizing Antibodies with Limited Somatic Mutation. *Immunity* **53**, 98-105
950 e105, doi:10.1016/j.immuni.2020.06.001 (2020).
951 15 Yuan, M. *et al*. Structural basis of a shared antibody response to SARS-CoV-2. *Science*
952 *(New York, N.Y.)* **369**, 1119-1123, doi:10.1126/science.abd2321 (2020).
953 16 Weisblum, Y. *et al*. Escape from neutralizing antibodies by SARS-CoV-2 spike protein
954 variants. *Elife* **9**, doi:10.7554/eLife.61312 (2020).
955 17 Barnes, C. O. *et al*. SARS-CoV-2 neutralizing antibody structures inform therapeutic
956 strategies. *Nature*, 1-25, doi:10.1038/s41586-020-2852-1 (2020).

957 18 Tortorici, M. A. *et al*. Ultrapotent human antibodies protect against SARS-CoV-2
958 challenge via multiple mechanisms. *Science (New York, N.Y.)* **4**, eabe3354-3316,
959 doi:10.1126/science.abe3354 (2020).
960 19 Baum, A. *et al*. Antibody cocktail to SARS-CoV-2 spike protein prevents rapid
961 mutational escape seen with individual antibodies. *Science (New York, N.Y.)* **369**, 1014-
962 1018, doi:10.1126/science.abd0831 (2020).
963 20 Li, Q. *et al*. The Impact of Mutations in SARS-CoV-2 Spike on Viral Infectivity and
964 Antigenicity. *Cell* **182**, 1284-1294 e1289, doi:10.1016/j.cell.2020.07.012 (2020).
965 21 Lamers, M. M. *et al*. SARS-CoV-2 productively infects human gut enterocytes. *Science*
966 *(New York, N.Y.)* **369**, 50-54, doi:10.1126/science.abc1669 (2020).
967 22 Livanos, A. E. *et al*. Gastrointestinal involvement attenuates COVID-19 severity and
968 mortality. *medRxiv*, 1-52, doi:10.1101/2020.09.07.20187666 (2020).
969 23 Qian, Q. *et al*. Direct evidence of active SARS-CoV-2 replication in the intestine. *Clin*
970 *Infect Dis*, 1-6, doi:10.1093/cid/ciaa925 (2020).
971 24 Han, Y. *et al*. Identification of SARS-CoV-2 Inhibitors using Lung and Colonic
972 Organoids. *Nature*, doi:10.1038/s41586-020-2901-9 (2020).
973 25 Morone, G. *et al*. Incidence and Persistence of Viral Shedding in COVID-19 Post-acute
974 Patients With Negativized Pharyngeal Swab: A Systematic Review. *Front Med*
975 *(Lausanne)* **7**, 562, doi:10.3389/fmed.2020.00562 (2020).
976 26 Park, S. K. *et al*. Detection of SARS-CoV-2 in Fecal Samples From Patients With
977 Asymptomatic and Mild COVID-19 in Korea. *Clin Gastroenterol Hepatol*, 1-11,
978 doi:10.1016/j.cgh.2020.06.005 (2020).
979 27 Wolfel, R. *et al*. Virological assessment of hospitalized patients with COVID-2019.
980 *Nature* **581**, 465-469, doi:10.1038/s41586-020-2196-x (2020).
981 28 Beaudoin-Bussieres, G. *et al*. Decline of Humoral Responses against SARS-CoV-2 Spike
982 in Convalescent Individuals. *mBio* **11**, 398-397, doi:10.1128/mBio.02590-20 (2020).
983 29 Crawford, K. H. D. *et al*. Dynamics of neutralizing antibody titers in the months after
984 SARS-CoV-2 infection. *J Infect Dis*, 1-15, doi:10.1093/infdis/jiaa618 (2020).
985 30 Iyer, A. S. *et al*. Persistence and decay of human antibody responses to the receptor
986 binding domain of SARS-CoV-2 spike protein in COVID-19 patients. *Sci Immunol* **5**,
987 eabe0367-0313, doi:10.1126/sciimmunol.abe0367 (2020).
988 31 Wang, K. *et al*. Longitudinal dynamics of the neutralizing antibody response to SARS-
989 CoV-2 infection. *Clin Infect Dis* **579**, 270-279, doi:10.1093/cid/ciaa1143 (2020).
990 32 Schafer, A. *et al*. Antibody potency, effector function and combinations in protection
991 from SARS-CoV-2 infection in vivo. *bioRxiv* **182**, 828-826,
992 doi:10.1101/2020.09.15.298067 (2020).
993 33 Ripperger, T. J. *et al*. Orthogonal SARS-CoV-2 Serological Assays Enable Surveillance
994 of Low Prevalence Communities and Reveal Durable Humoral Immunity. *Immunity*, 1-
995 49, doi:10.1016/j.immuni.2020.10.004 (2020).
996 34 Dan, J. M. *et al*. Immunological memory to SARS-CoV-2 assessed for greater than six
997 months after infection. *bioRxiv*, 2020.2011.2015.383323, doi:10.1101/2020.11.15.383323
998 (2020).
999 35 Rodda, L. B. *et al*. Functional SARS-CoV-2-specific immune memory persists after mild
1000 COVID-19. *medRxiv*, doi:10.1101/2020.08.11.20171843 (2020).

1001 36 Secchi, M. *et al*. COVID-19 survival associates with the immunoglobulin response to the
1002 SARS-CoV-2 spike receptor binding domain. *J Clin Invest* **130**, doi:10.1172/JCI142804
1003 (2020).
1004 37 Liu, L. *et al*. Potent neutralizing antibodies against multiple epitopes on SARS-CoV-2
1005 spike. *Nature* **584**, 450-456, doi:10.1038/s41586-020-2571-7 (2020).
1006 38 Zost, S. J. *et al*. Potently neutralizing and protective human antibodies against SARS-
1007 CoV-2. *Nature* **584**, 443-449, doi:10.1038/s41586-020-2548-6 (2020).
1008 39 Nielsen, S. C. A. *et al*. Human B Cell Clonal Expansion and Convergent Antibody
1009 Responses to SARS-CoV-2. *Cell host & microbe* **28**, 516-525 e515,
1010 doi:10.1016/j.chom.2020.09.002 (2020).
1011 40 Kaneko, N. *et al*. Loss of Bcl-6-Expressing T Follicular Helper Cells and Germinal
1012 Centers in COVID-19. *Cell* **183**, 143-157 e113, doi:10.1016/j.cell.2020.08.025 (2020).
1013 41 Victora, G. D. & Nussenzweig, M. C. Germinal centers. *Annu Rev Immunol* **30**, 429-457,
1014 doi:10.1146/annurev-immunol-020711-075032 (2012).
1015 42 Sokal, A. *et al*. Maturation and persistence of the anti-SARS-CoV-2 memory B cell
1016 response. *bioRxiv*, 2020.2011.2017.385252, doi:10.1101/2020.11.17.385252 (2020).
1017 43 Mahler, D. A. & Wells, C. K. Evaluation of clinical methods for rating dyspnea. *Chest*
1018 **93**, 580-586, doi:10.1378/chest.93.3.580 (1988).
1019 44 Pujadas, E. *et al*. SARS-CoV-2 viral load predicts COVID-19 mortality. *The Lancet*.
1020 *Respiratory medicine* **8**, e70, doi:10.1016/S2213-2600(20)30354-4 (2020).
1021 45 Chomczynski, P. & Sacchi, N. Single-step method of RNA isolation by acid guanidinium
1022 thiocyanate-phenol-chloroform extraction. *Analytical biochemistry* **162**, 156-159,
1023 doi:10.1006/abio.1987.9999 (1987).
1024 46 DeAngelis, M. M., Wang, D. G. & Hawkins, T. L. Solid-phase reversible immobilization
1025 for the isolation of PCR products. *Nucleic Acids Res* **23**, 4742-4743,
1026 doi:10.1093/nar/23.22.4742 (1995).
1027 47 Grifoni, A. *et al*. Targets of T Cell Responses to SARS-CoV-2 Coronavirus in Humans
1028 with COVID-19 Disease and Unexposed Individuals. *Cell* **181**, 1489-1501 e1415,
1029 doi:10.1016/j.cell.2020.05.015 (2020).
1030 48 Amanat, F. *et al*. A serological assay to detect SARS-CoV-2 seroconversion in humans.
1031 *Nat Med* **26**, 1033-1036, doi:10.1038/s41591-020-0913-5 (2020).
1032 49 Barnes, C. O. *et al*. Structures of Human Antibodies Bound to SARS-CoV-2 Spike
1033 Reveal Common Epitopes and Recurrent Features of Antibodies. *Cell* **182**, 828-842 e816,
1034 doi:10.1016/j.cell.2020.06.025 (2020).
1035 50 Schmidt, F. *et al*. Measuring SARS-CoV-2 neutralizing antibody activity using
1036 pseudotyped and chimeric viruses. *J Exp Med* **217**, doi:10.1084/jem.20201181 (2020).
1037 51 Weisblum, Y. *et al*. Escape from neutralizing antibodies by SARS-CoV-2 spike protein
1038 variants. *bioRxiv* **17**, 1055-1042, doi:10.1101/2020.07.21.214759 (2020).
1039 52 Van Gassen, S. *et al*. FlowSOM: Using self-organizing maps for visualization and
1040 interpretation of cytometry data. *Cytometry*. *Part A : the journal of the International*
1041 *Society for Analytical Cytology* **87**, 636-645, doi:10.1002/cyto.a.22625 (2015).
1042 53 Gupta, N. T. *et al*. Change-O: a toolkit for analyzing large-scale B cell immunoglobulin
1043 repertoire sequencing data. *Bioinformatics (Oxford, England)* **31**, 3356-3358,
1044 doi:10.1093/bioinformatics/btv359 (2015).
1045 54 Soto, C. *et al*. High frequency of shared clonotypes in human B cell receptor repertoires.
1046 *Nature* **566**, 398-402, doi:10.1038/s41586-019-0934-8 (2019).

1047 55 Guo, Y., Chen, K., Kwong, P. D., Shapiro, L. & Sheng, Z. cAb-Rep: A Database of
1048 Curated Antibody Repertoires for Exploring Antibody Diversity and Predicting Antibody
1049 Prevalence. *Front Immunol* **10**, 2365, doi:10.3389/fimmu.2019.02365 (2019).
1050 56 Kyte, J. & Doolittle, R. F. A simple method for displaying the hydropathic character of a
1051 protein. *J Mol Biol* **157**, 105-132, doi:10.1016/0022-2836(82)90515-0 (1982).
1052 57 Guy, H. R. Amino acid side-chain partition energies and distribution of residues in
1053 soluble proteins. *Biophysical journal* **47**, 61-70, doi:10.1016/S0006-3495(85)83877-7
1054 (1985).
1055 58 DeWitt, W. S. *et al*. A Public Database of Memory and Naive B-Cell Receptor
1056 Sequences. *PLoS One* **11**, e0160853, doi:10.1371/journal.pone.0160853 (2016).
1057 59 Spiegel, M. *et al*. Inhibition of Beta interferon induction by severe acute respiratory
1058 syndrome coronavirus suggests a two-step model for activation of interferon regulatory
1059 factor 3. *J Virol* **79**, 2079-2086, doi:10.1128/JVI.79.4.2079-2086.2005 (2005).
1060

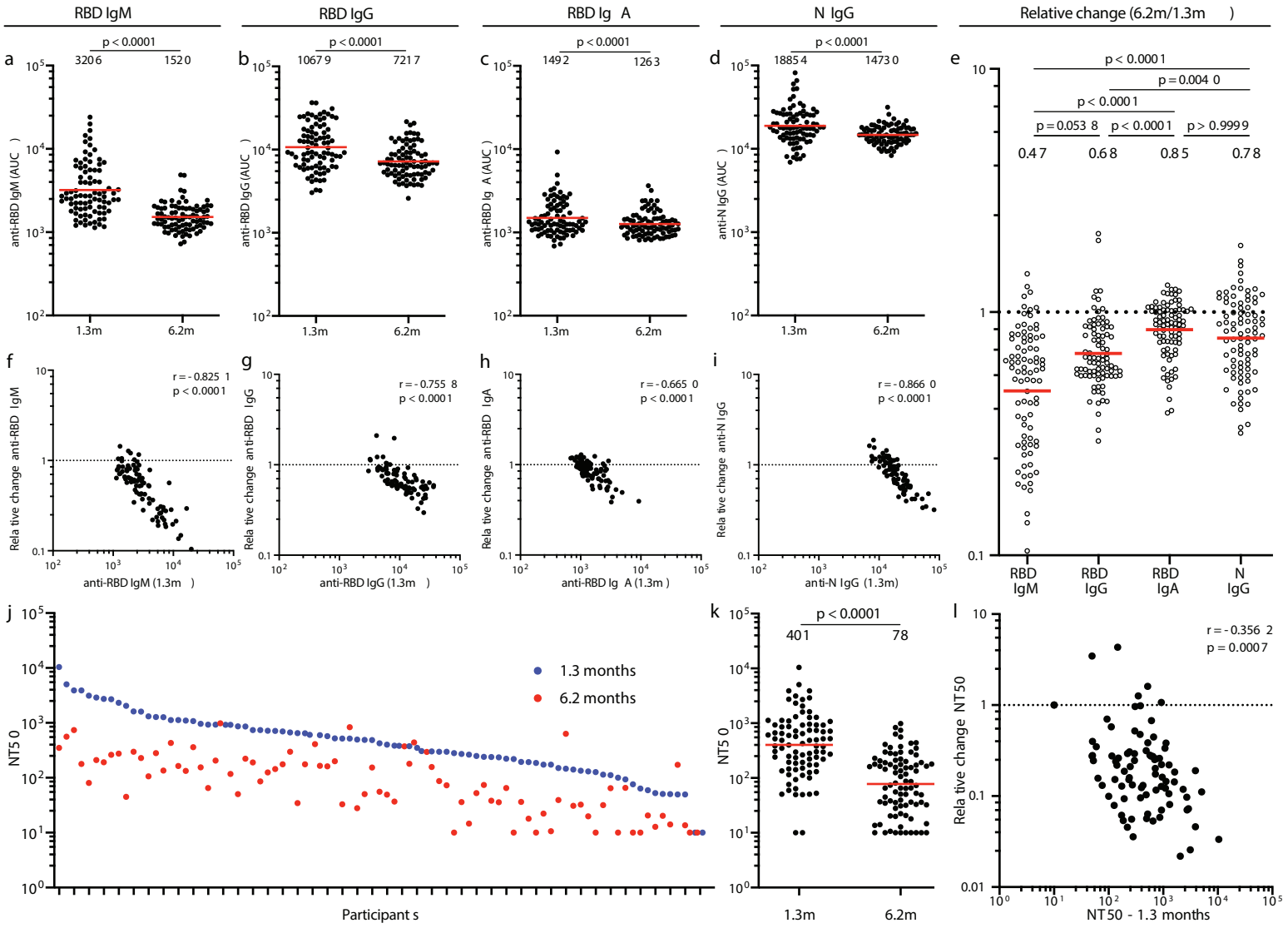
RBD IgM
RBD IgG
RBD Ig A
N IgG
Relative change (6.2m/1.3m)
a
b
c
d
e
p < 0.0001
3206
1520
10679
7217
1492
1263
18854
14730
anti-RBD IgM (AUC)
anti-RBD IgG (AUC)
anti-RBD Ig A (AUC)
anti-N IgG (AUC)
1.3m
6.2m
p < 0.0001
p = 0.0040
p = 0.0538
p > 0.9999
0.47
0.68
0.85
0.78
RBD IgM
RBD IgG
RBD IgA
N IgG
f
g
h
i
r = -0.8251
r = -0.7558
r = -0.6650
r = -0.8660
Relative change anti-RBD IgM
Relative change anti-RBD IgG
Relative change anti-RBD IgA
Relative change anti-N IgG
anti-RBD IgM (1.3m)
anti-RBD IgG (1.3m)
anti-RBD Ig A (1.3m)
anti-N IgG (1.3m)
j
k
l
1.3 months
6.2 months
NT50
Participants
401
78
r = -0.3562
p = 0.0007
Relative change NT50
NT50 - 1.3 months

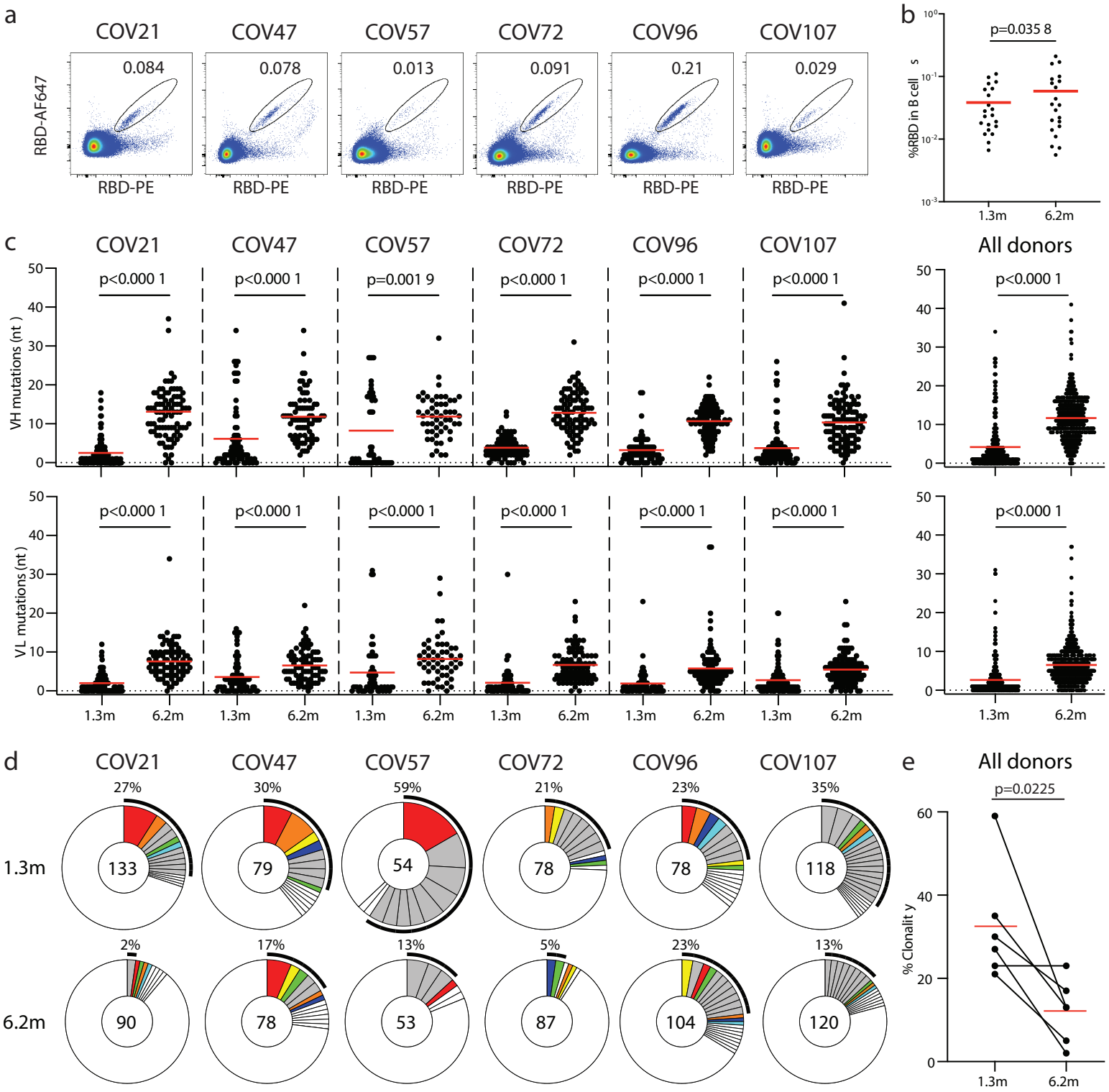
a
COV21
COV47
COV57
COV72
COV96
COV107
RBD-AF647
RBD-PE
0.084
0.078
0.013
0.091
0.21
0.029
b
p=0.035 8
%RBD in B cell s
1.3m
6.2m
c
All donors
VH mutations (nt)
VL mutations (nt)
p<0.000 1
p=0.001 9
d
27%
30%
59%
21%
23%
35%
133
79
54
78
78
118
2%
17%
13%
5%
23%
13%
90
78
53
87
104
120
e
p=0.0225
% Clonality

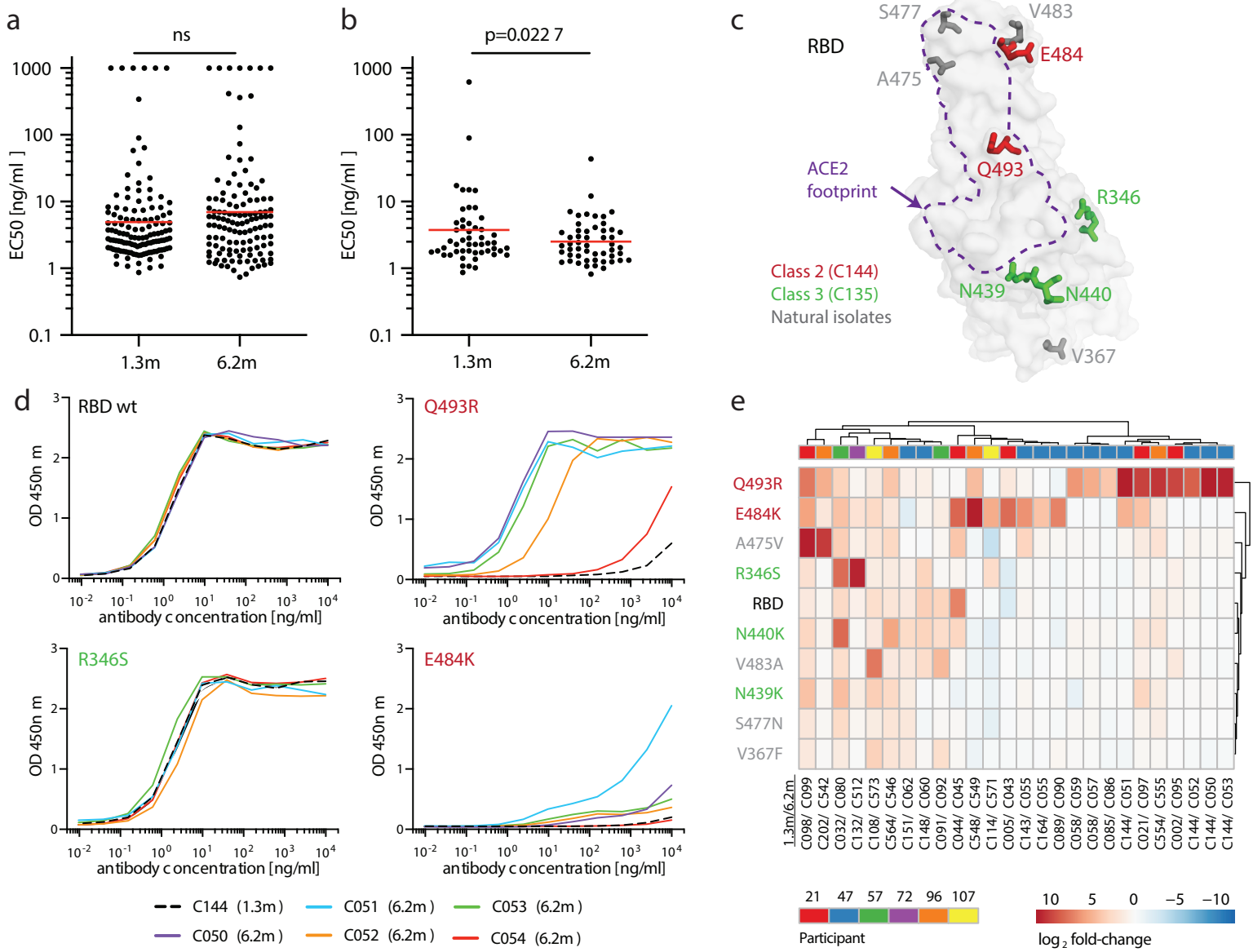
a
ns
EC50 [ng/ml]
1000
100
10
1
0.1
1.3m
6.2m
b
p=0.022 7
EC50 [ng/ml]
1000
100
10
1
0.1
1.3m
6.2m
c
RBD
S477
V483
E484
A475
Q493
ACE2
footprint
R346
Class 2 (C144)
Class 3 (C135)
Natural isolates
N439
N440
V367
d
RBD wt
Q493R
R346S
E484K
OD 450n m
antibody c oncentration [ng/ml]
C144 (1.3m)
C051 (6.2m)
C053 (6.2m)
C050 (6.2m)
C052 (6.2m)
C054 (6.2m)
e
Q493R
E484K
A475V
R346S
RBD
N440K
V483A
N439K
S477N
V367F
1.3m/6.2m
C098/ C099
C202/ C542
C032/ C080
C132/ C512
C108/ C573
C564/ C546
C151/ C062
C148/ C060
C091/ C092
C044/ C045
C548/ C549
C114/ C571
C005/ C043
C143/ C055
C164/ C055
C089/ C090
C058/ C059
C058/ C057
C085/ C086
C144/ C051
C021/ C097
C554/ C555
C002/ C095
C144/ C052
C144/ C050
C144/ C053
21 47 57 72 96 107
Participant
10 5 0 −5 −10
log 2 fold-change

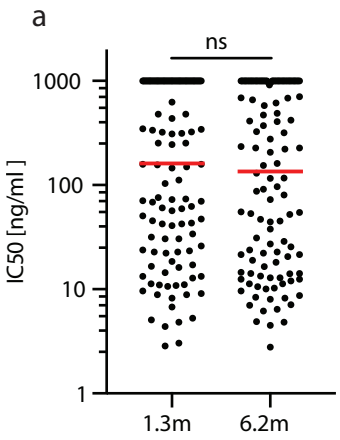

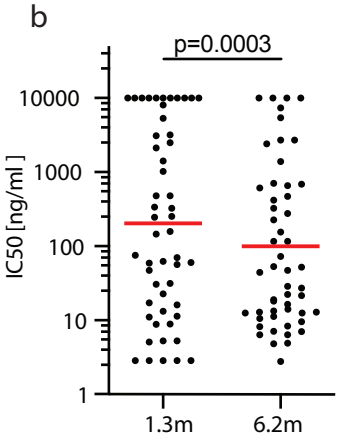

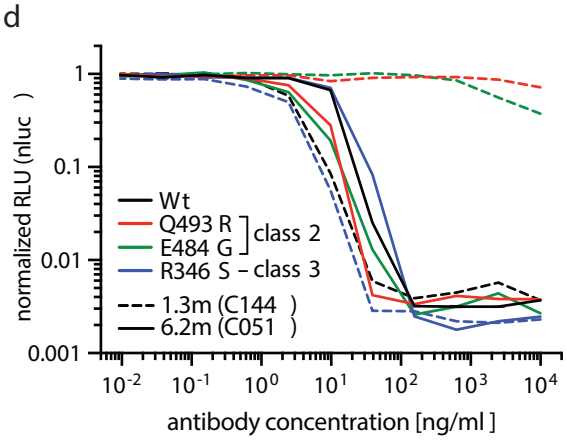

c

	IC 50 [ng/ml]			
	wt	Q493 R	E 484 G	R 346 S
C144	2.73	>1000 0	4114 .07	1.78
C051	11.99	4.68	3.10	13.56
C548	19.13	>1000 0	1591 .77	10.84
C549	10.95	2.35	2.29	8.33
C032	100 .69	62.42	45.68	>1000 0
C080	21.52	21.25	6.00	5.31
C132	1024 .35	796 .48	1406 .57	>1000 0
C512	21.55	20.78	12.17	4022 .02
C164	87.89	139.53	369.18	57.24
C143	191 .23	1576 .12	4402 .39	224.99
C055	4.98	6.52	44.78	4.03

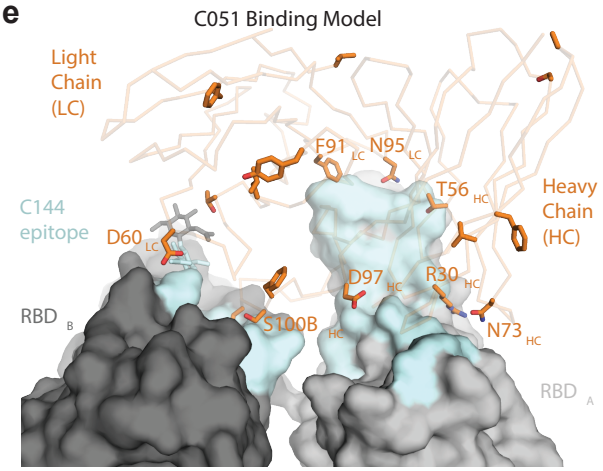

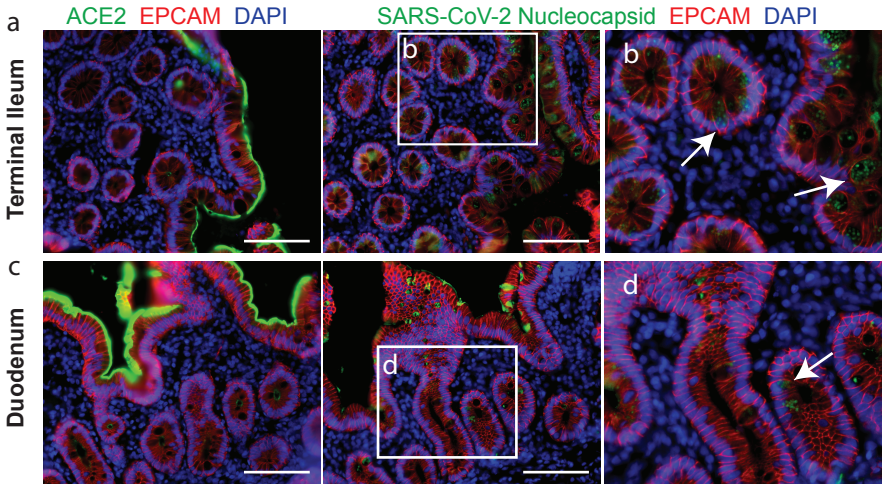
a
ACE2 EPCAM DAPI
SARS-CoV-2 Nucleocapsid EPCAM DAPI
Terminal Ileum
b
b
c
Duodenum
d
d

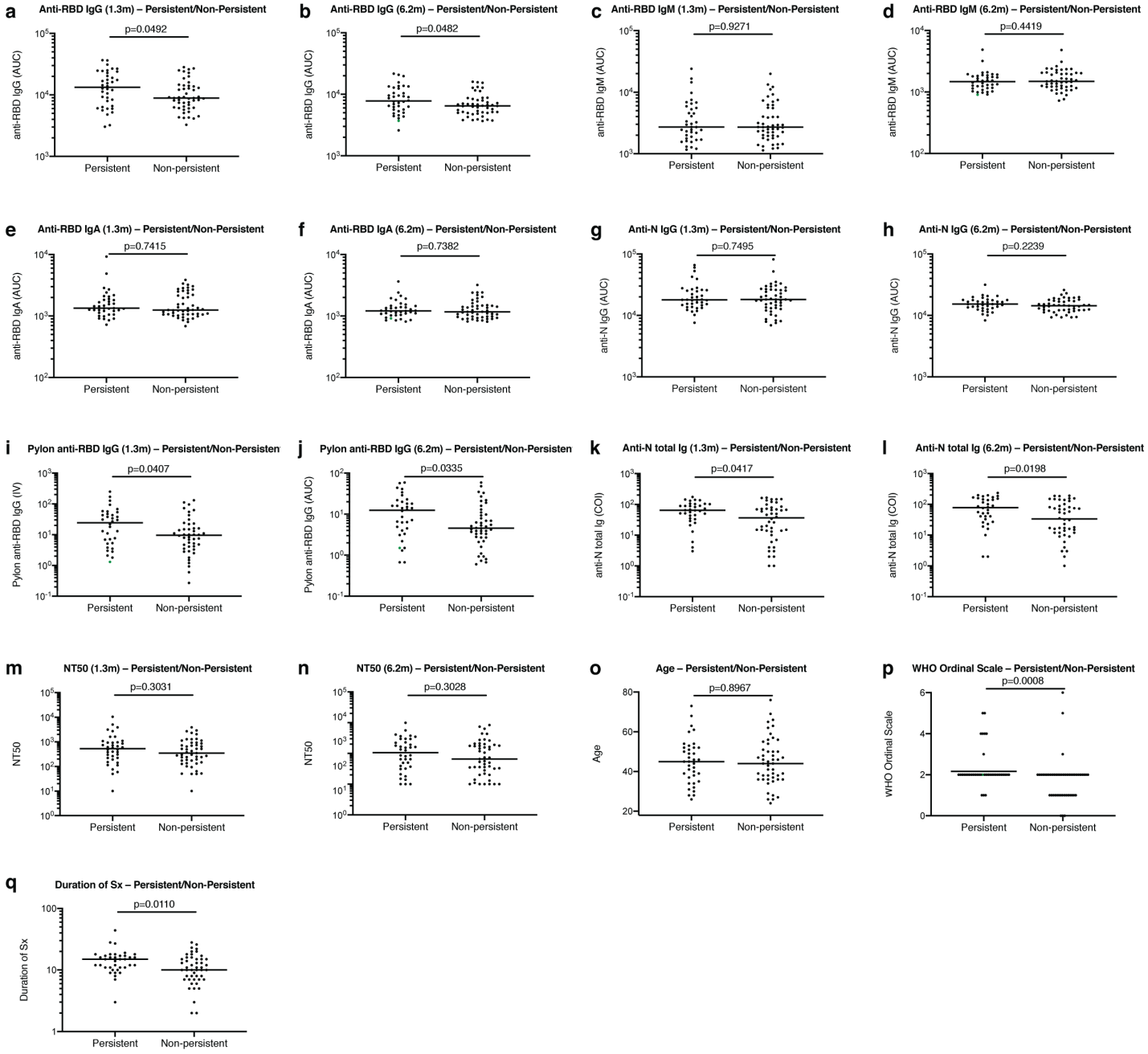
a
Anti-RBD IgG (1.3m) – Persistent/Non-Persistent
p=0.0492
anti-RBD IgG (AUC)
Persistent
Non-persistent
b
Anti-RBD IgG (6.2m) – Persistent/Non-Persistent
p=0.0482
anti-RBD IgG (AUC)
Persistent
Non-persistent
c
Anti-RBD IgM (1.3m) – Persistent/Non-Persistent
p=0.9271
anti-RBD IgM (AUC)
Persistent
Non-persistent
d
Anti-RBD IgM (6.2m) – Persistent/Non-Persistent
p=0.4419
anti-RBD IgM (AUC)
Persistent
Non-persistent
e
Anti-RBD IgA (1.3m) – Persistent/Non-Persistent
p=0.7415
anti-RBD IgA (AUC)
Persistent
Non-persistent
f
Anti-RBD IgA (6.2m) – Persistent/Non-Persistent
p=0.7382
anti-RBD IgA (AUC)
Persistent
Non-persistent
g
Anti-N IgG (1.3m) – Persistent/Non-Persistent
p=0.7495
anti-N IgG (AUC)
Persistent
Non-persistent
h
Anti-N IgG (6.2m) – Persistent/Non-Persistent
p=0.2239
anti-N IgG (AUC)
Persistent
Non-persistent
i
Pylon anti-RBD IgG (1.3m) – Persistent/Non-Persisten
p=0.0407
Pylon anti-RBD IgG (IV)
Persistent
Non-persistent
j
Pylon anti-RBD IgG (6.2m) – Persistent/Non-Persisten
p=0.0335
Pylon anti-RBD IgG (AUC)
Persistent
Non-persistent
k
Anti-N total Ig (1.3m) – Persistent/Non-Persistent
p=0.0417
anti-N total Ig (COI)
Persistent
Non-persistent
l
Anti-N total Ig (6.2m) – Persistent/Non-Persistent
p=0.0198
anti-N total Ig (COI)
Persistent
Non-persistent
m
NT50 (1.3m) – Persistent/Non-Persistent
p=0.3031
NT50
Persistent
Non-persistent
n
NT50 (6.2m) – Persistent/Non-Persistent
p=0.3028
NT50
Persistent
Non-persistent
o
Age – Persistent/Non-Persistent
p=0.8967
Age
Persistent
Non-persistent
p
WHO Ordinal Scale – Persistent/Non-Persistent
p=0.0008
WHO Ordinal Scale
Persistent
Non-persistent
q
Duration of Sx – Persistent/Non-Persistent
p=0.0110
Duration of Sx
Persistent
Non-persistent

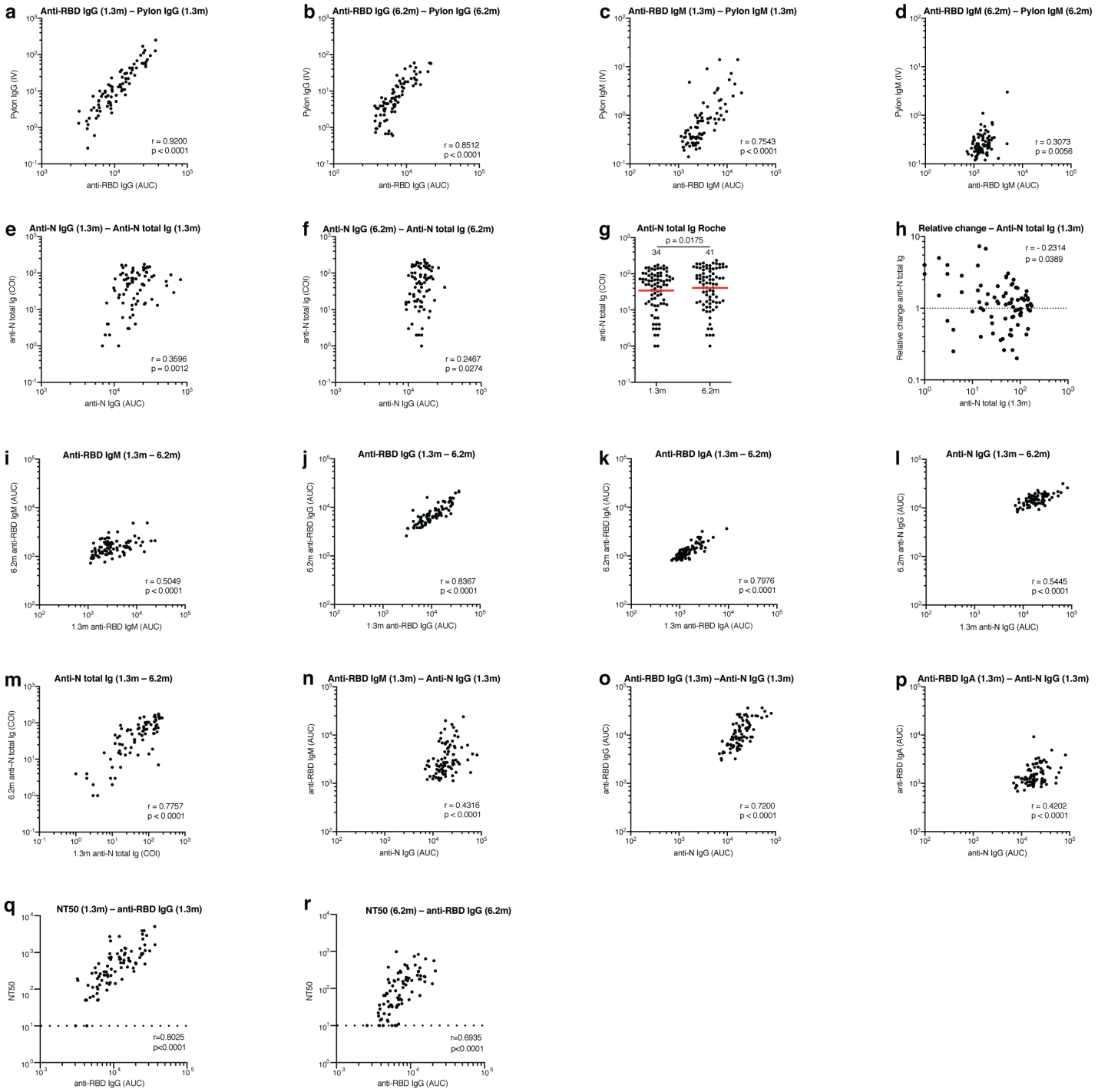
a
Anti-RBD IgG (1.3m) – Pylon IgG (1.3m)
Pylon IgG (IV)
anti-RBD IgG (AUC)
r = 0.9200
p < 0.0001
b
Anti-RBD IgG (6.2m) – Pylon IgG (6.2m)
Pylon IgG (IV)
anti-RBD IgG (AUC)
r = 0.8512
p < 0.0001
c
Anti-RBD IgM (1.3m) – Pylon IgM (1.3m)
Pylon IgM (IV)
anti-RBD IgM (AUC)
r = 0.7543
p < 0.0001
d
Anti-RBD IgM (6.2m) – Pylon IgM (6.2m)
Pylon IgM (IV)
anti-RBD IgM (AUC)
r = 0.3073
p = 0.0056
e
Anti-N IgG (1.3m) – Anti-N total Ig (1.3m)
anti-N total Ig (COI)
anti-N IgG (AUC)
r = 0.3596
p = 0.0012
f
Anti-N IgG (6.2m) – Anti-N total Ig (6.2m)
anti-N total Ig (COI)
anti-N IgG (AUC)
r = 0.2467
p = 0.0274
g
Anti-N total Ig Roche
p = 0.0175
34
41
anti-N total Ig (COI)
1.3m
6.2m
h
Relative change – Anti-N total Ig (1.3m)
Relative change anti-N total Ig
anti-N total Ig (1.3m)
r = - 0.2314
p = 0.0389
i
Anti-RBD IgM (1.3m – 6.2m)
6.2m anti-RBD IgM (AUC)
1.3m anti-RBD IgM (AUC)
r = 0.5049
p < 0.0001
j
Anti-RBD IgG (1.3m – 6.2m)
6.2m anti-RBD IgG (AUC)
1.3m anti-RBD IgG (AUC)
r = 0.8367
p < 0.0001
k
Anti-RBD IgA (1.3m – 6.2m)
6.2m anti-RBD IgA (AUC)
1.3m anti-RBD IgA (AUC)
r = 0.7976
p < 0.0001
l
Anti-N IgG (1.3m – 6.2m)
6.2m anti-N IgG (AUC)
1.3m anti-N IgG (AUC)
r = 0.5445
p < 0.0001
m
Anti-N total Ig (1.3m – 6.2m)
6.2m anti-N total Ig (COI)
1.3m anti-N total Ig (COI)
r = 0.7757
p < 0.0001
n
Anti-RBD IgM (1.3m) – Anti-N IgG (1.3m)
anti-RBD IgM (AUC)
anti-N IgG (AUC)
r = 0.4316
p < 0.0001
o
Anti-RBD IgG (1.3m) –Anti-N IgG (1.3m)
anti-RBD IgG (AUC)
anti-N IgG (AUC)
r = 0.7200
p < 0.0001
p
Anti-RBD IgA (1.3m) – Anti-N IgG (1.3m)
anti-RBD IgA (AUC)
anti-N IgG (AUC)
r = 0.4202
p < 0.0001
q
NT50 (1.3m) – anti-RBD IgG (1.3m)
NT50
anti-RBD IgG (AUC)
r=0.8025
p<0.0001
r
NT50 (6.2m) – anti-RBD IgG (6.2m)
NT50
anti-RBD IgG (AUC)
r=0.6935
p<0.0001

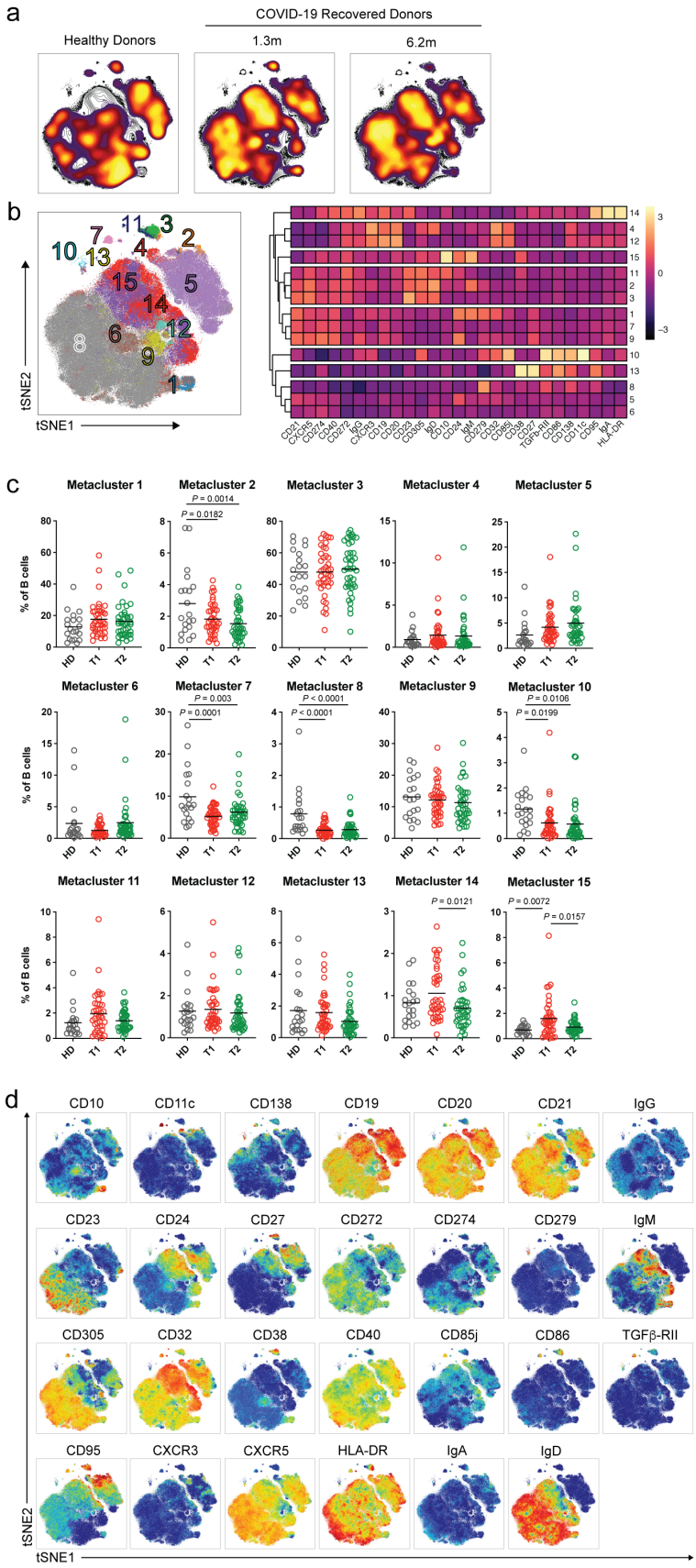
a
COVID-19 Recovered Donors
Healthy Donors
1.3m
6.2m
b
tSNE2
tSNE1
CD21
CXCR5
CD274
CD40
CD272
IgG
CXCR3
CD19
CD20
CD23
CD305
IgD
CD10
CD24
IgM
CD279
CD32
CD85j
CD38
CD27
TGFb-RII
CD86
CD138
CD11c
CD95
IgA
HLA-DR
c
Metacluster 1
Metacluster 2
Metacluster 3
Metacluster 4
Metacluster 5
Metacluster 6
Metacluster 7
Metacluster 8
Metacluster 9
Metacluster 10
Metacluster 11
Metacluster 12
Metacluster 13
Metacluster 14
Metacluster 15
% of B cells
HD
T1
T2
P = 0.0014
P = 0.0182
P = 0.003
P = 0.0001
P < 0.0001
P < 0.0001
P = 0.0106
P = 0.0199
P = 0.0121
P = 0.0072
P = 0.0157
d
CD10
CD11c
CD138
CD19
CD20
CD21
IgG
CD23
CD24
CD27
CD272
CD274
CD279
IgM
CD305
CD32
CD38
CD40
CD85j
CD86
TGFβ-RII
CD95
CXCR3
CXCR5
HLA-DR
IgA
IgD
tSNE2
tSNE1

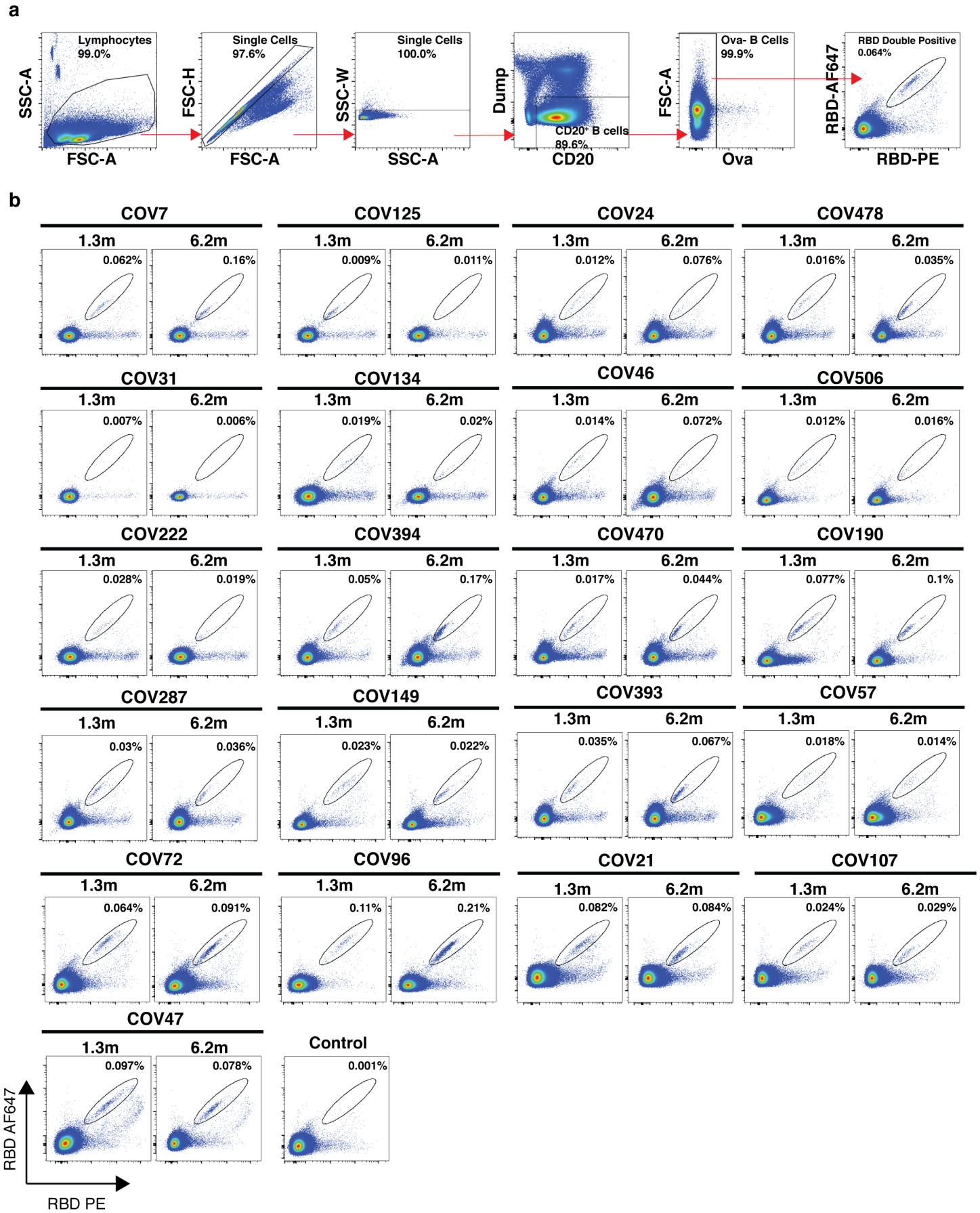
a
Lymphocytes
99.0%
SSC-A
FSC-A
Single Cells
97.6%
FSC-H
FSC-A
Single Cells
100.0%
SSC-W
SSC-A
Dump
CD20+ B cells
89.6%
CD20
FSC-A
Ova- B Cells
99.9%
Ova
RBD Double Positive
0.064%
RBD-AF647
RBD-PE
b
COV7
1.3m 0.062%
6.2m 0.16%
COV125
1.3m 0.009%
6.2m 0.011%
COV24
1.3m 0.012%
6.2m 0.076%
COV478
1.3m 0.016%
6.2m 0.035%
COV31
1.3m 0.007%
6.2m 0.006%
COV134
1.3m 0.019%
6.2m 0.02%
COV46
1.3m 0.014%
6.2m 0.072%
COV506
1.3m 0.012%
6.2m 0.016%
COV222
1.3m 0.028%
6.2m 0.019%
COV394
1.3m 0.05%
6.2m 0.17%
COV470
1.3m 0.017%
6.2m 0.044%
COV190
1.3m 0.077%
6.2m 0.1%
COV287
1.3m 0.03%
6.2m 0.036%
COV149
1.3m 0.023%
6.2m 0.022%
COV393
1.3m 0.035%
6.2m 0.067%
COV57
1.3m 0.018%
6.2m 0.014%
COV72
1.3m 0.064%
6.2m 0.091%
COV96
1.3m 0.11%
6.2m 0.21%
COV21
1.3m 0.082%
6.2m 0.084%
COV107
1.3m 0.024%
6.2m 0.029%
COV47
1.3m 0.097%
6.2m 0.078%
Control
0.001%
RBD AF647
RBD PE

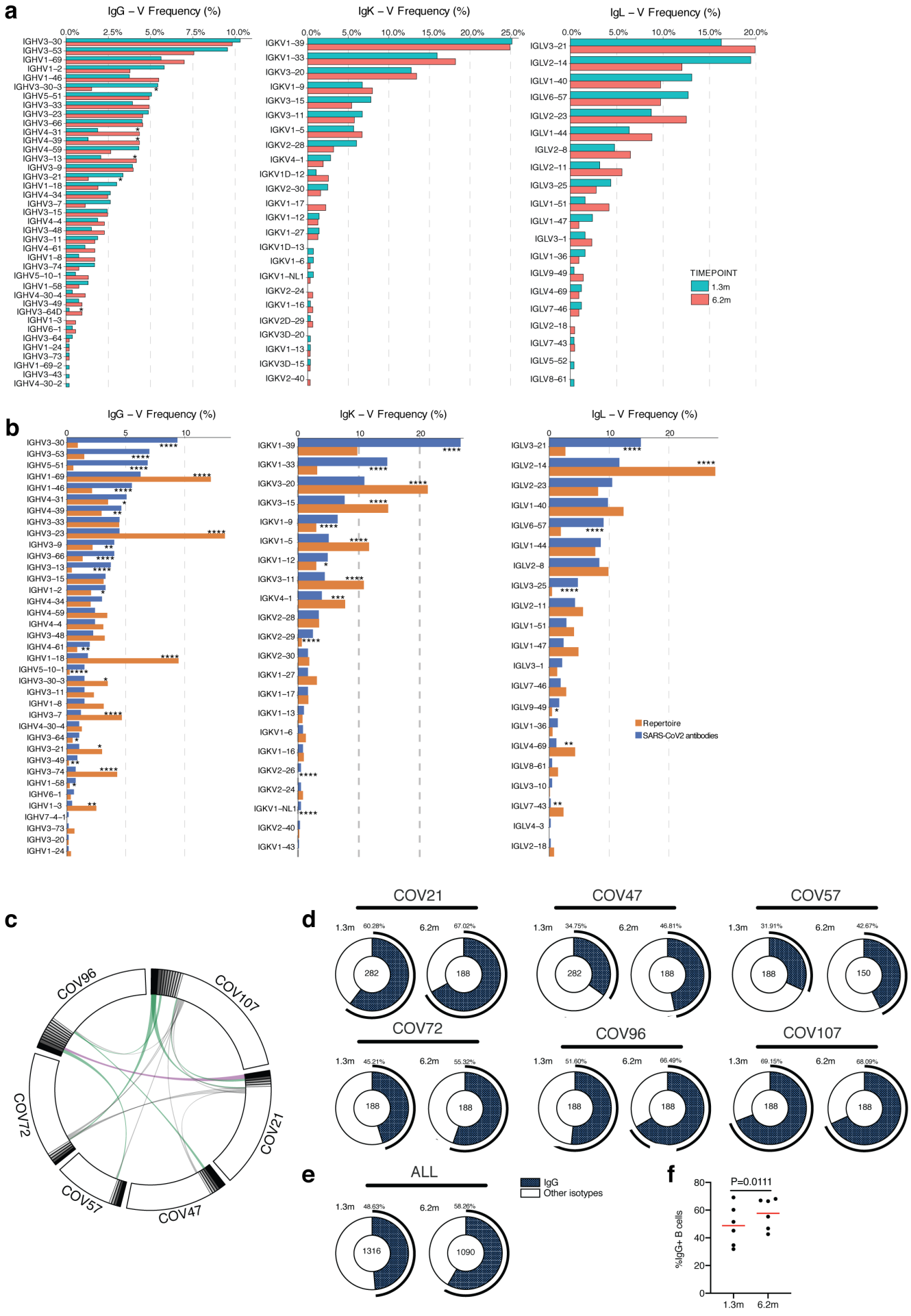
a
IgG – V Frequency (%)
IgK – V Frequency (%)
IgL – V Frequency (%)
TIMEPOINT
1.3m
6.2m
b
IgG – V Frequency (%)
IgK – V Frequency (%)
IgL – V Frequency (%)
Repertoire
SARS-CoV2 antibodies
c
COV96
COV107
COV72
COV21
COV57
COV47
d
COV21
COV47
COV57
COV72
COV96
COV107
1.3m
6.2m
e
ALL
IgG
Other isotypes
1316
1090
f
P=0.0111
%IgG+ B cells
1.3m
6.2m

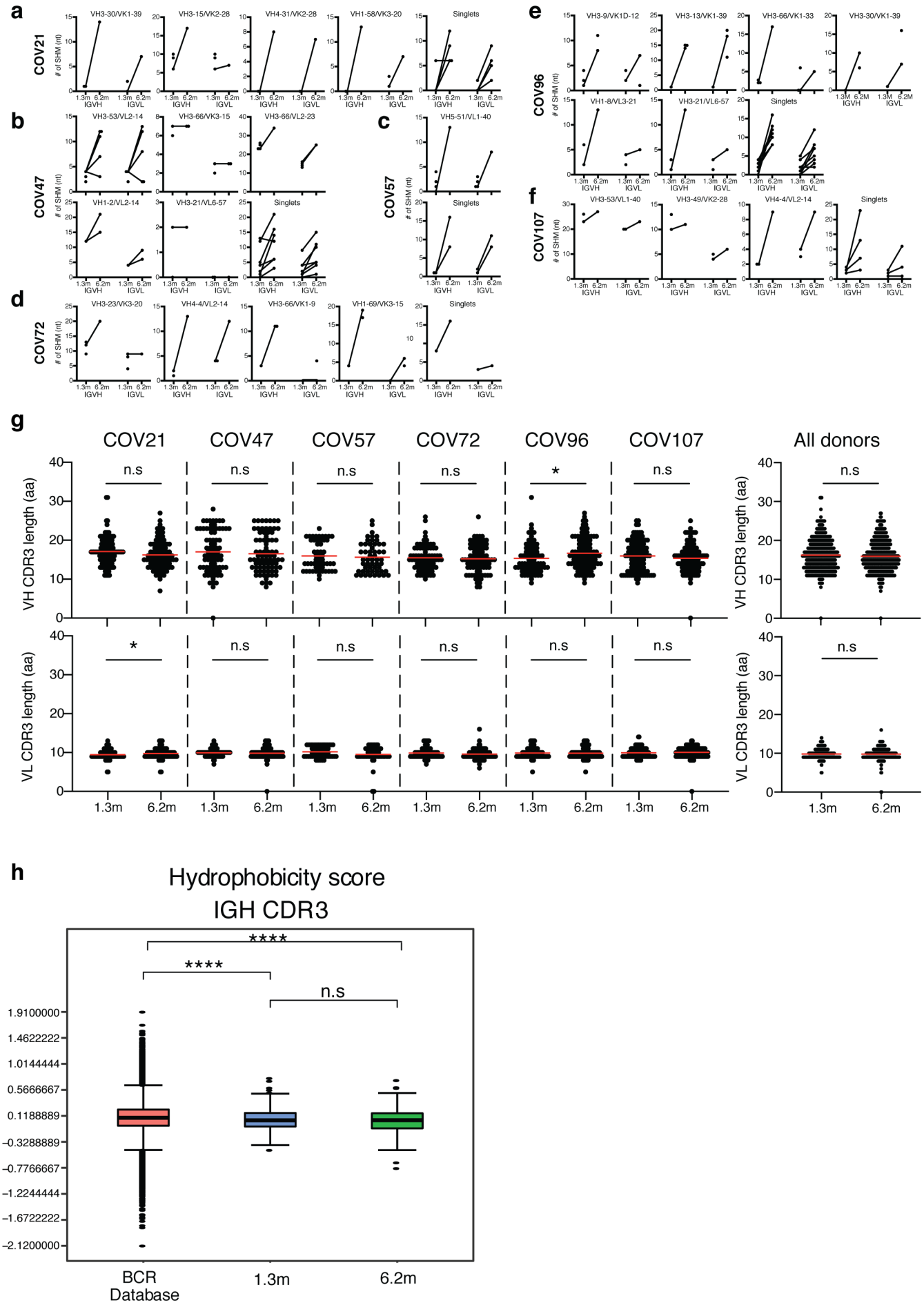
a
COV21
VH3-30/VK1-39
VH3-15/VK2-28
VH4-31/VK2-28
VH1-58/VK3-20
Singlets
b
COV47
VH3-53/VL2-14
VH3-66/VK3-15
VH3-66/VL2-23
VH1-2/VL2-14
VH3-21/VL6-57
Singlets
c
COV57
VH5-51/VL1-40
Singlets
d
COV72
VH3-23/VK3-20
VH4-4/VL2-14
VH3-66/VK1-9
VH1-69/VK3-15
Singlets
e
COV96
VH3-9/VK1D-12
VH3-13/VK1-39
VH3-66/VK1-33
VH3-30/VK1-39
VH1-8/VL3-21
VH3-21/VL6-57
Singlets
f
COV107
VH3-53/VL1-40
VH3-49/VK2-28
VH4-4/VL2-14
Singlets
# of SHM (nt)
IGVH
IGVL
1.3m
6.2m
g
COV21
COV47
COV57
COV72
COV96
COV107
All donors
VH CDR3 length (aa)
VL CDR3 length (aa)
n.s
*
h
Hydrophobicity score
IGH CDR3
GRAVY score
****
n.s
BCR Database
1.3m
6.2m

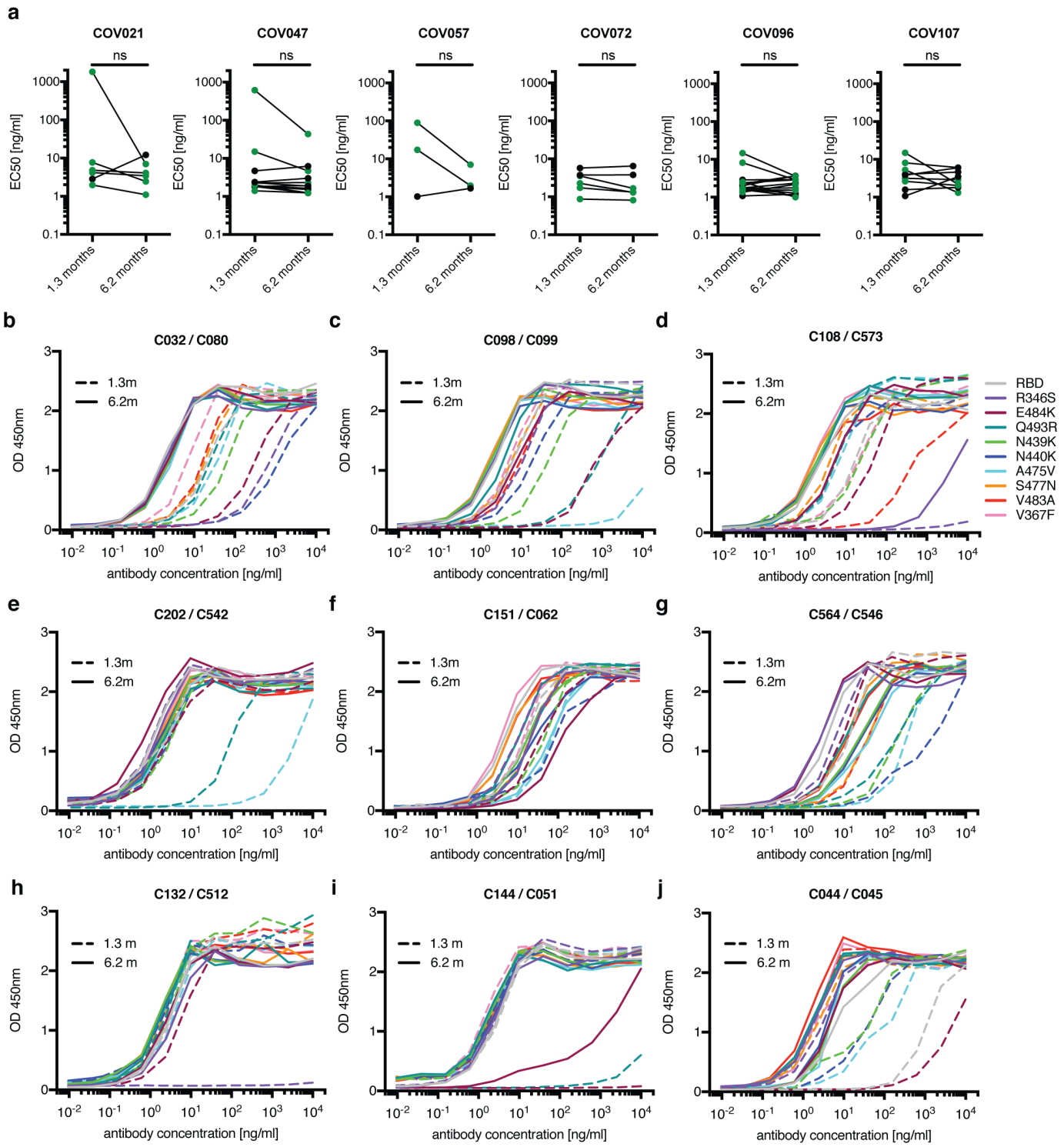
a
COV021
COV047
COV057
COV072
COV096
COV107
ns
EC50 [ng/ml]
1.3 months
6.2 months
b
C032 / C080
c
C098 / C099
d
C108 / C573
e
C202 / C542
f
C151 / C062
g
C564 / C546
h
C132 / C512
i
C144 / C051
j
C044 / C045
1.3m
6.2m
OD 450nm
antibody concentration [ng/ml]
RBD
R346S
E484K
Q493R
N439K
N440K
A475V
S477N
V483A
V367F

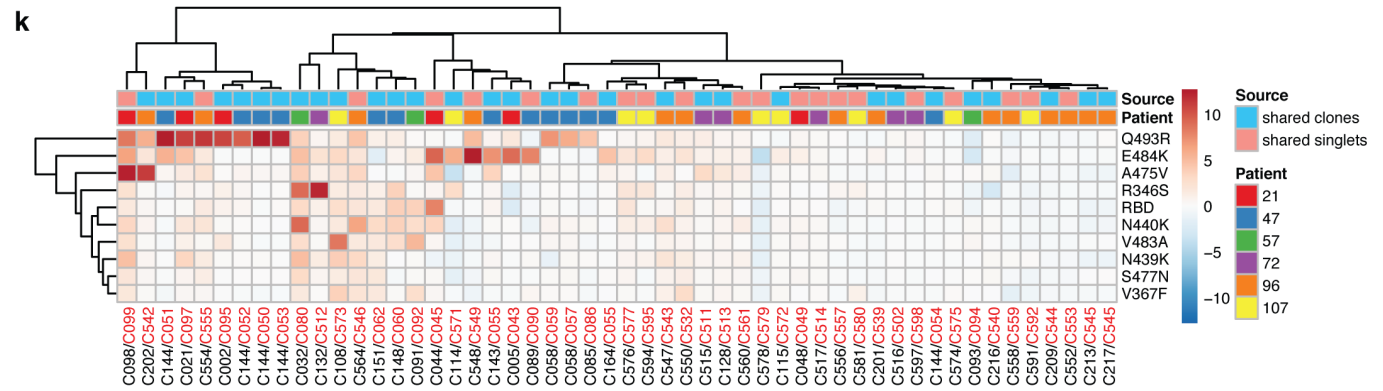
k
Source
Patient
Q493R
E484K
A475V
R346S
RBD
N440K
V483A
N439K
S477N
V367F
Source
shared clones
shared singlets
Patient
21
47
57
72
96
107

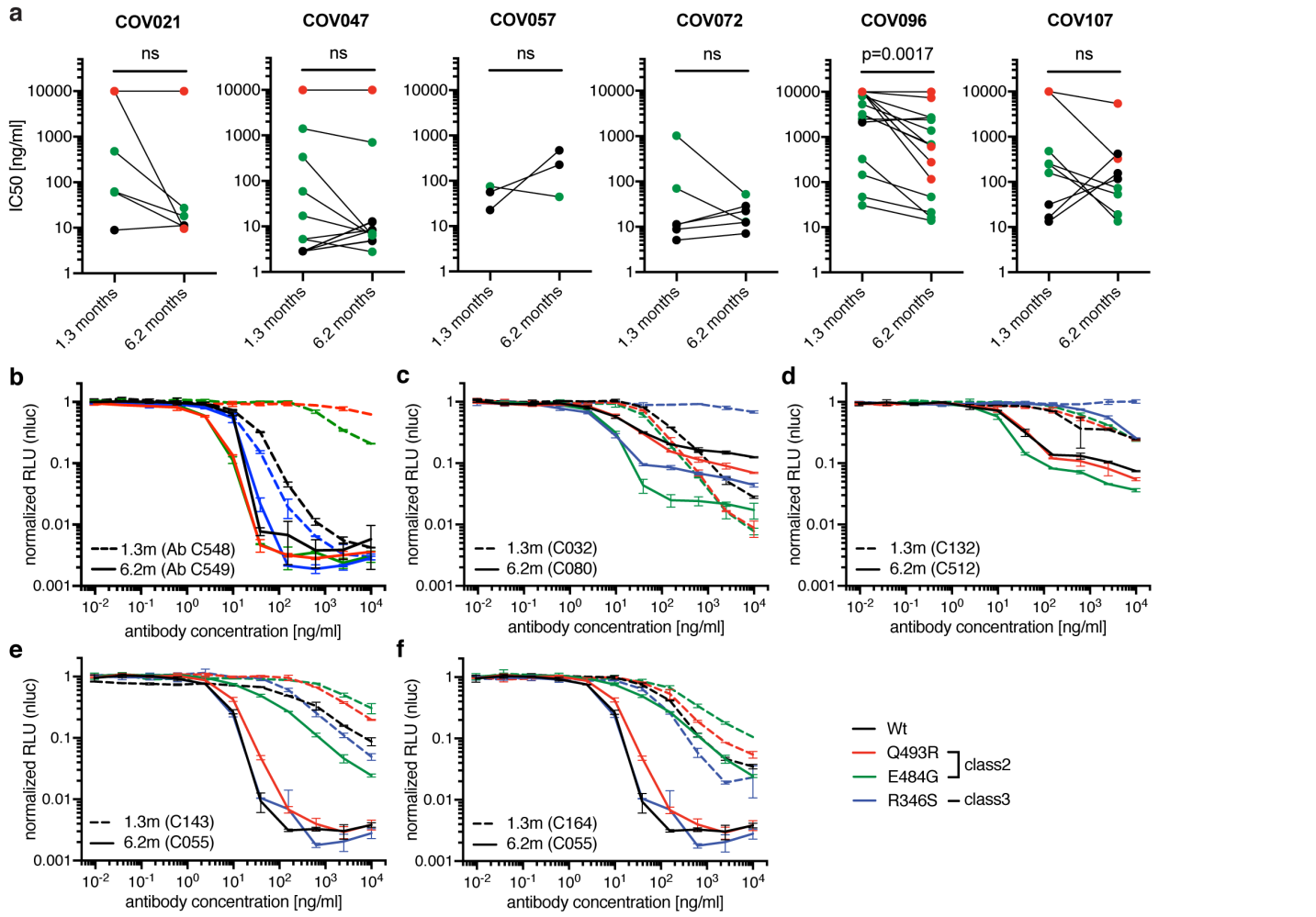
a
COV021
COV047
COV057
COV072
COV096
COV107
ns
p=0.0017
IC50 [ng/ml]
1.3 months
6.2 months
b
c
d
e
f
normalized RLU (nluc)
antibody concentration [ng/ml]
1.3m (Ab C548)
6.2m (Ab C549)
1.3m (C032)
6.2m (C080)
1.3m (C132)
6.2m (C512)
1.3m (C143)
6.2m (C055)
1.3m (C164)
6.2m (C055)
Wt
Q493R
E484G
class2
R346S
class3

g

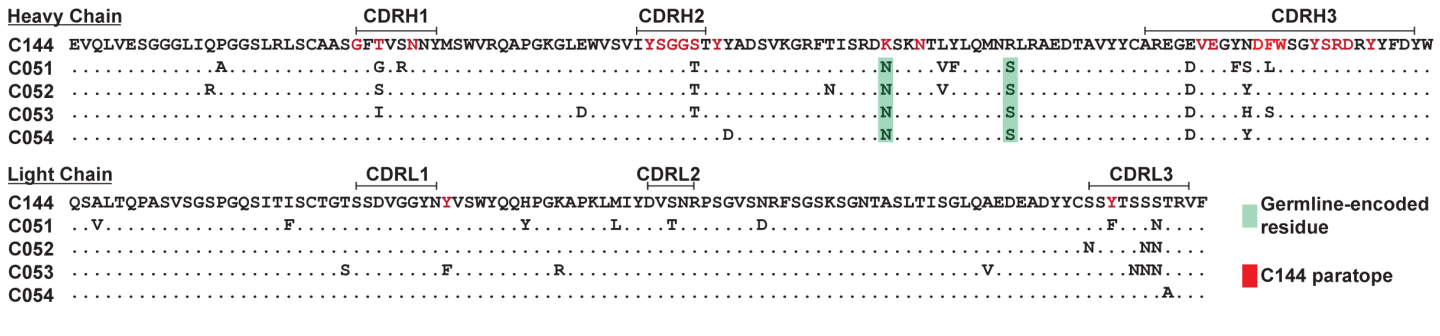
Heavy Chain
CDRH1
CDRH2
CDRH3
C144 EVQLVESGGGLIQPGGSLRLSCAASGFTVSNNYMSWVRQAPGKGLEWVSVIYSGGSTYYADSVKGRFTISRDKSKNTLYLQMNRLRAEDTAVYYCAREGEVEGYNDFWSGYSRDRYYFDYW
C051
C052
C053
C054
Light Chain
CDRL1
CDRL2
CDRL3
C144 QSALTQPASVSGSPGQSITISCTGTSSDVGGYNYVSWYQQHPGKAPKLMIYDVSNRPSGVSNRFSGSKSGNTASLTISGLQAEDEADYYCSSYTSSSTRVF
C051
C052
C053
C054
Germline-encoded residue
C144 paratope

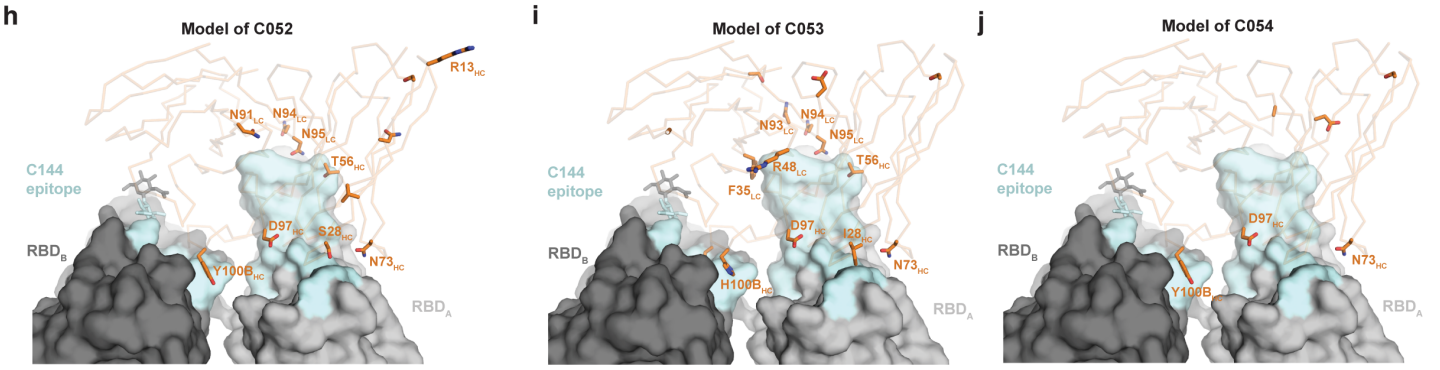
h
Model of C052
i
Model of C053
j
Model of C054
C144 epitope
RBD_B
RBD_A
R13_HC
N91_LC
N94_LC
N95_LC
T56_HC
D97_HC
S28_HC
N73_HC
Y100B_HC
N93_LC
R48_LC
F35_LC
I28_HC
H100B_HC

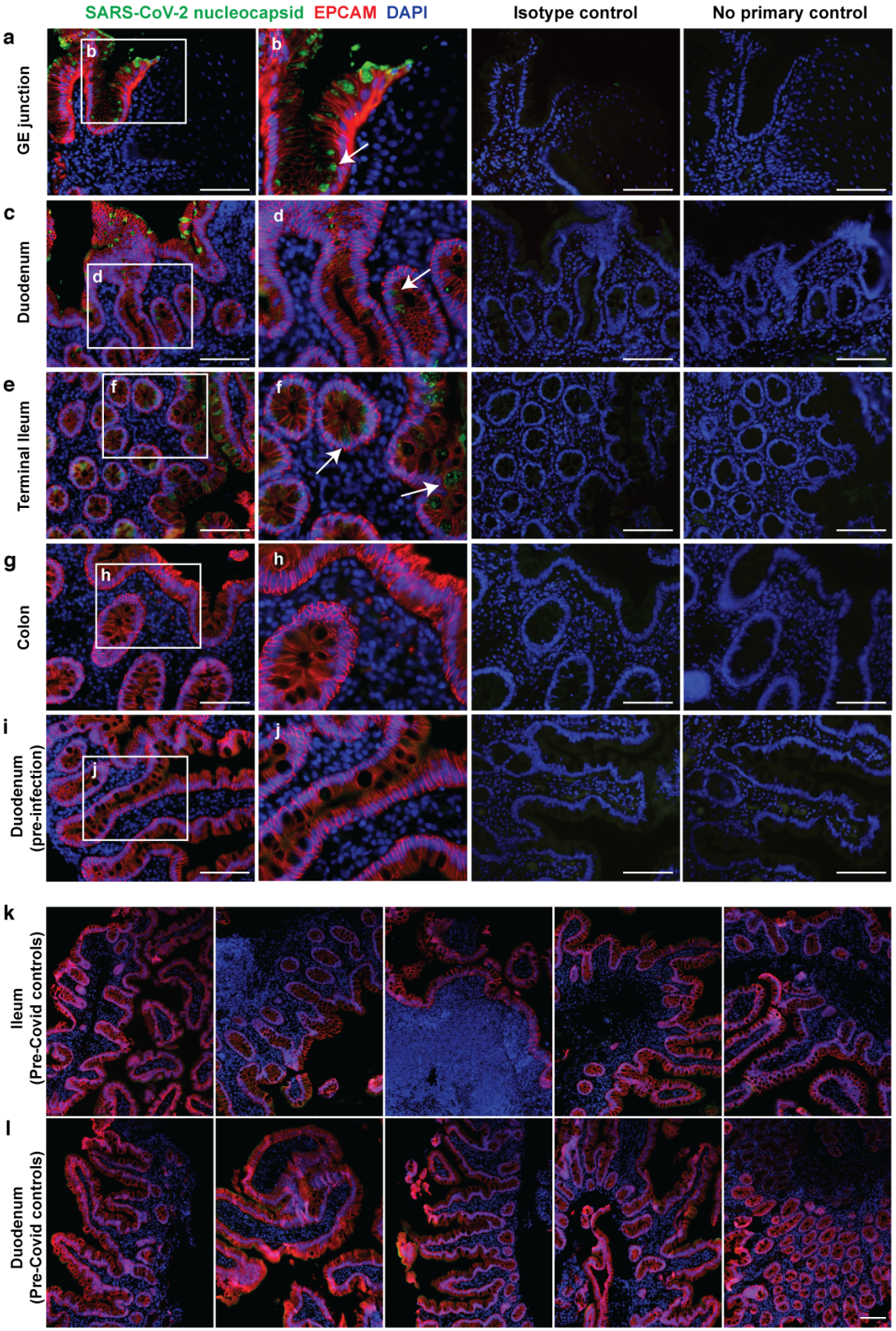
SARS-CoV-2 nucleocapsid EPCAM DAPI
Isotype control
No primary control
a
GE junction
b
b
c
Duodenum
d
d
e
Terminal Ileum
f
f
g
Colon
h
h
i
Duodenum (pre-infection)
j
j
k
Ileum (Pre-Covid controls)
l
Duodenum (Pre-Covid controls)

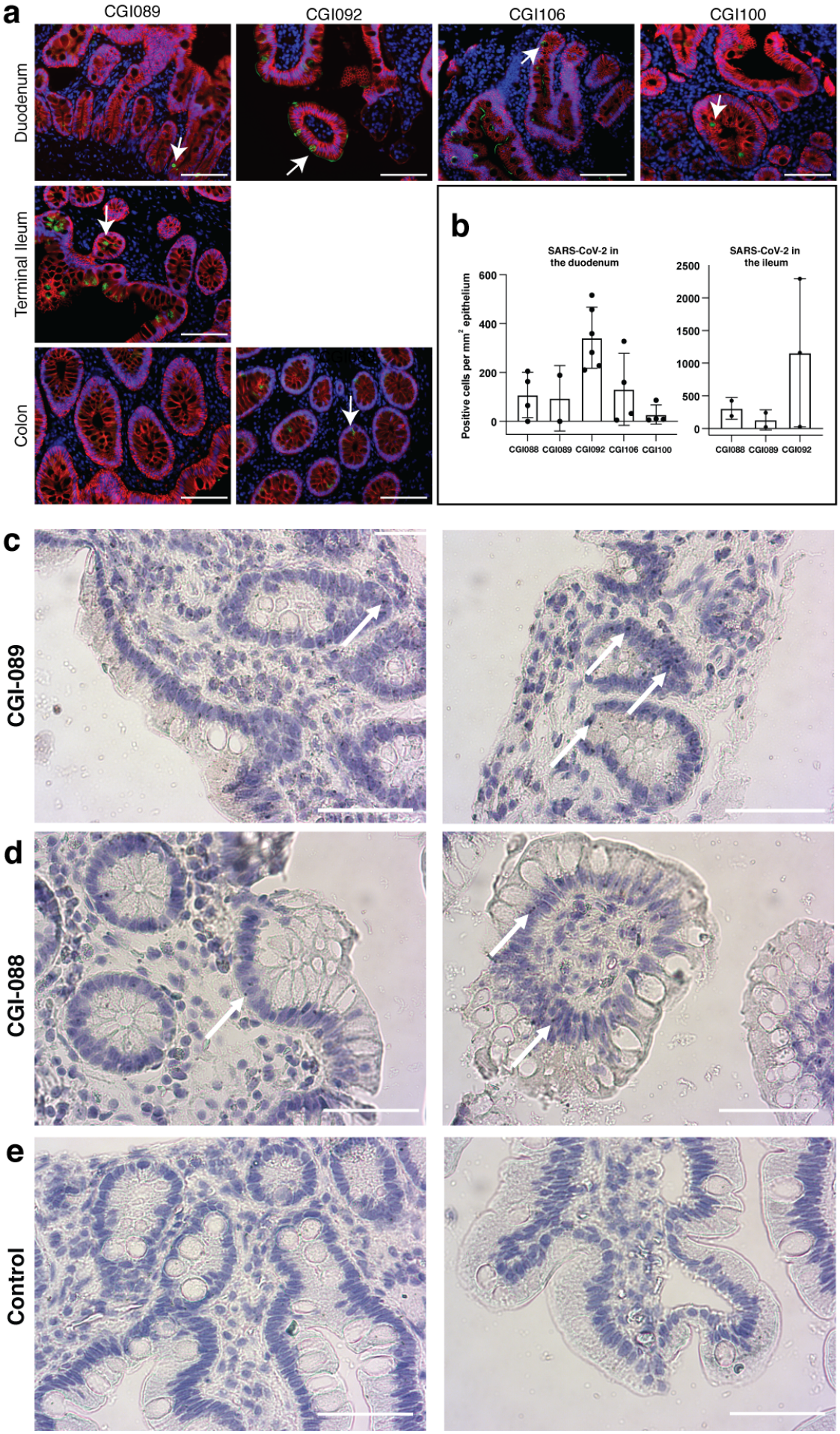
a
CGI089
CGI092
CGI106
CGI100
Duodenum
Terminal Ileum
Colon
b
SARS-CoV-2 in the duodenum
SARS-CoV-2 in the ileum
Positive cells per mm² epithelium
600
400
200
0
2500
2000
1500
1000
500
0
CGI088
CGI089
CGI092
CGI106
CGI100
c
CGI-089
d
CGI-088
e
Control